SAND REPORT
SAND2002-3779
Unlimited Release
Printed November 2002

Effect of Weather on the Predicted PMN Landmine Chemical Signature for Kabul, Afghanistan

Stephen W. Webb and James M. Phelan

Prepared by
Sandia National Laboratories
Albuquerque, New Mexico 87185 and Livermore, California 94550

Sandia is a multiprogram laboratory operated by Sandia Corporation, a Lockheed Martin Company, for the United States Department of Energy under Contract DE-AC04-94AL85000.

Sandia National Laboratories

Issued by Sandia National Laboratories, operated for the United States Department of Energy by Sandia Corporation.

Available to DOE and DOE contractors from
U.S. Department of Energy
Office of Scientific and Technical Information
P.O. Box 62
Oak Ridge, TN 37831

Telephone: (865)576-8401
Facsimile: (865)576-5728
E-Mail: reports@adonis.osti.gov
Online ordering: http://www.doe.gov/bridge

Available to the public from
U.S. Department of Commerce
National Technical Information Service
5285 Port Royal Rd
Springfield, VA 22161

Telephone: (800)553-6847
Facsimile: (703)605-6900
E-Mail: orders@ntis.fedworld.gov
Online order: http://www.ntis.gov/help/ordermethods.asp?loc=7-4-0#online

SAND2002-3779
Unlimited Release
Printed November 2002

Effect of Weather on the Predicted PMN Landmine Chemical Signature for Kabul, Afghanistan

Stephen W. Webb and James M. Phelan
Environmental Technology Department
Sandia National Laboratories
P.O. Box 5800
Albuquerque, NM, USA, 87185-0719

Abstract

Buried landmines are often detected through the chemical signature in the air above the soil surface by mine detection dogs. Environmental processes play a significant role in the chemical signature available for detection. Due to the shallow burial depth of landmines, the weather influences the release of chemicals from the landmine, transport through the soil to the surface, and degradation processes in the soil. The effect of weather on the landmine chemical signature from a PMN landmine was evaluated with the T2TNT code for Kabul, Afghanistan. Results for TNT and DNT gas-phase and soil solid-phase concentrations are presented as a function of time of the day and time of the year.

Table of Contents

List of Figures

List of Tables

Nomenclature

A,B,C	empirical constants (-)
A	$\log_{10} K_d$' (-)
A_0	$\log_{10} K_d$' ($w_m = 0.$) (-)
c	cloud cover (-)
c_p	specific heat (J/kg-K)
d	displacement height (m)
D	diffusivity (m^2/s)
E	evaporation mass flux (kg/m^2-s)
f_{VPL}	vapor pressure lowering factor (-)
H	heat flux (W/m^2)
J	day of year (-)
k	von Karmen constant (=0.4)
k_r	relative permeability (-)
K_d	distribution coefficient for liquid-solid sorption (mL/g)
K_d'	distribution coefficient for gas-solid sorption at zero liquid saturation (mL/g)
K_E	effective distribution coefficient (mL/g)
K_H	Henry's Law constant
K_{VS}	distribution coefficient for vapor-solid sorption (mL/g)
L	Monin-Obukhov length (m)
m,n	van Genuchten fitting parameters (-)
m_l	molecular weight of water (kg/kg-mole)
P	pressure (Pa)
P_c	capillary pressure (Pa)
P_{sat}	saturation pressure (Pa)
P_v	vapor pressure (Pa)
R	radiation emittance (-); resistance (s/m)
RH	relative humidity (-)
S	liquid saturation (-)
$S_{l,r}$	liquid residual saturation (-)
S_l	liquid saturation (-)
S_t	solar radiation at ground surface (W/m^2)
S_{ext}	solar constant (1367 W/m^2)
t	time (s)
t_d	time of day (hr)
t_o	solar noon (hr)
T	temperature (K, ^oC)
T_t	transmission coefficient (-)
ΔT	temperature difference, maximum temperature minus minimum temperature, (K)
u*	friction velocity (m/s)
U	velocity (m/s)
w_m	mass moisture content (-)
z	elevation above ground surface (m)
z_{oh}	roughness length for heat (m)
z_{om}	roughness length for momentum (m)

Greek

α	vapor-solid sorption parameter (-)
α_{vG}	air entry pressure parameter (1/Pa)
ρ	density (kg/m^3)
δ	boundary layer thickness (m), solar declination angle (radians)
ϕ	latitude (radians)
ε	emissivity (-)
τ	momentum flux ($kg/m\text{-}s^2$)
σ	Stefan-Boltzmann constant (=5.67 x 10^{-8} $W/m^2\text{-}K^4$)
ω	mass fraction (-)
Ψ_m	velocity profile function (-)
Ψ_h	temperature profile function (-)
α_{bg}	albedo of bare ground (-)
ε_g	emissivity of ground (-)

Subscripts

a	air
amp	amplitude
av	average
aH	heat
aM	momentum
aV	water vapor
c	clear
e	effective
l	liquid
lw	long-wave
r	residual
s	surface, saturated
V	water vapor

Acknowledgments

The work was sponsored by the Geneva International Center for Humanitarian Demining (GICHD) under the direction of Havard Bach. Sandia is a multiprogram laboratory operated by Sandia Corporation, a Lockheed Martin Company, for the United States Department of Energy under Contract DE-AC04-94AL85000.

1.0 Introduction

1.1 Background

Trace chemical detection of buried landmines is a challenging task due to the extremely low concentrations available for sensing. Understanding the nature of the trace chemical detection process has matured through evaluation of the individual landmine-soil-atmosphere processes, and through evaluation of the interdependencies among these individual processes using sophisticated computer simulation tools (Phelan and Webb, 2002). The goal of this understanding is to define optimal conditions to field trace chemical detection activities and those indicating poor probability for success.

Computational simulation models articulate the fundamental processes mathematically to provide a representation of the emissions of the signature chemicals from the buried landmine, movements through the soil, and release at the ground surface. We must recognize that, while care has been taken to include most of the known processes and interdependencies, representations by computer simulations are not reality. Comparisons of simulation model predictions to laboratory data have been very good (Phelan et al., 2000, 2001), providing confidence that the model represents well the reality of certain situations. Thus, benefits from computer simulation exercises need to be recognized for use in guiding field campaigns and identifying weaknesses in our understanding of this challenging problem.

The present study investigates the impact of weather conditions on the movement of landmine signature chemicals through the subsurface and into the atmosphere. The situation modeled is for a single landmine typically found in Afghanistan (PMN) and the weather conditions typical for Kabul. The code used was T2TNT, with specific improvements since initial development (Webb et al., 1999). Weather data available for Kabul were incomplete, so methods were developed to estimate the missing parameters from available information. The T2TNT code currently does not include the effects of plants, so a bare soil version was used, which more appropriately mimics many locations in Afghanistan. The physical models in T2TNT important to landmine chemical movement are described in detail for a better understanding and interpretation of the results.

A similar study was performed for analysis of landmine chemical transport representing a landmine at the U.S. Army field test site at Ft. Leonard Wood, Missouri, USA (Webb and Phelan, 2000). The model is updated in the present case by inclusion of environmentally-dependent chemical degradation and mine flux source rate based on experimental data.

1.2 Environmental Processes

Environmental processes play a significant role in the chemical signature available for trace chemical detection by sensors or animals. Due to the shallow burial depth of landmines, the weather influences the release of chemicals from the landmine, transport through the soil to the surface, and degradation processes in the soil.

Figure 1 depicts the complex interdependencies affecting landmine chemical transport in the soil. Chemical vapors emanate from a buried landmine by permeation through the case materials

or leakage through seals and seams, and from surface contamination on the case. Transport through the surrounding soil occurs in the liquid and gas phases by diffusion and advection. Liquid phase advection is driven by precipitation and evaporation of water from the soil, and gas advection can occur due to barometric pressure changes. Partitioning among the phases is important for explosive compounds, which tends to concentrate the explosives on the solid and liquid phases. The explosive compounds are also subject to biotic and abiotic degradation.

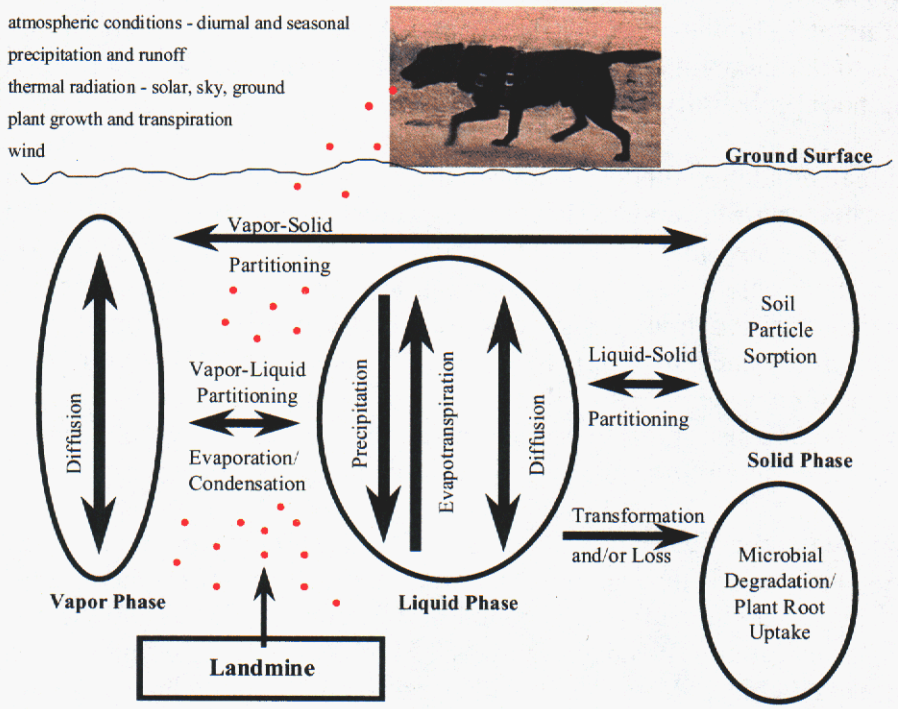

Figure 1.

Environmental Fate and Transport Processes for Chemical Detection of Buried Landmines.

Figure 2 depicts the principal environmental conditions at the ground surface. Wind has a direct effect on the transport of chemicals from the soil into the atmosphere. Thermal radiation, which consists of solar and long-wave components, impacts the surface and subsurface temperature. The atmospheric conditions (pressure, temperature, and relative humidity) affect gas phase transport to the surface, the surface air temperature, and water evaporation from the soil into the atmosphere. Precipitation and runoff directly influence soil moisture and chemical movement in the liquid and gas phases. The soil temperature and moisture content affect the degradation of the chemicals in the soil. Finally, plant growth and transpiration impact the net transport of radiation to the soil surface, the net water infiltration into the soil, the air-atmosphere transition region, and act as sinks for subsurface water and dissolved chemicals. Phelan and Webb (2002) discuss these factors in more detail.

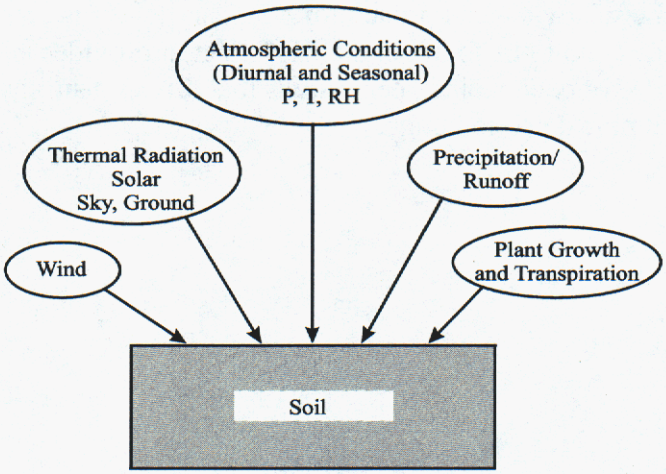

Figure 2.
Land Surface Boundary Conditions

1.3 Environmental Factors at the Soil-Atmosphere Interface

The soil-atmosphere interface is a region, or boundary layer, where landmine signature chemical concentrations rapidly change from the value at the soil surface to essentially zero in the atmosphere. It is in this region that landmine signature chemicals are sensed by trace chemical detection methods including sensors and dogs. In this region, significant changes in temperature, wind speed, water vapor, and chemical concentrations occur.

The T2TNT code uses steady-state boundary layer methodology to represent the soil-atmosphere interface. The water vapor and chemical concentration model considers the water vapor (evaporation) boundary layer, which is generally a thin (~1-10 cm) layer of air at the soil surface where the water vapor concentration changes from the value at the land surface to the value in the atmosphere. Within this water vapor boundary layer is a thinner (~0.25–2.5 cm) chemical boundary layer where the chemical concentration decreases from the value at the soil surface to a value of zero in the atmosphere. Values in the boundary layer change from the value adjacent to the surface to that in the atmosphere above the boundary layer in a highly non-linear manner.

The steady-state approach used in the T2TNT code is computationally efficient, but it does not include some phenomena due to the assumption of steady-state conditions. During unstable conditions when the soil is warmer than the air, which especially occurs on sunny days, transient phenomena are important as described by Settles and Kester (2001). Unstable thermal convection may occur, and local thermals can periodically transport landmine chemicals vertically into the atmosphere at much greater distances than the steady-state chemical boundary layer thickness. Modeling of these phenomena requires sophisticated computational fluid dynamics approaches and is computationally intensive.

While the simplicity of the steady-state approach for boundary layers is convenient, it may not represent well many of the conditions found in the field. Yet, it provides an initial understanding of the magnitude of chemical concentrations that drive sensitivity requirements for advanced technology and mine detection dogs.

2.0 Model Description

2.1 Weather Data

Weather data were obtained from NCAR (National Center for Atmospheric Research, Boulder, Colorado) for all the reporting weather stations in Afghanistan. The specific data set is at http://dss.ucar.edu/datasets/ds512.0. The data consist of entries for daily maximum and minimum temperature, precipitation, vapor pressure, evapotranspiration, minimum and maximum relative humidity, sea level pressure, snowfall, descriptive weather, cloud cover, wind direction, and wind speed. Radiation data (solar and long-wave) are not included in the data set. Cloud cover, snowfall, wind direction, and wind speed are not included prior to January 1994.

The weather station at Kabul, WMO identifier 40948, at an elevation of 1791 m was selected from the data set. There are almost no data after 1992, and the data earlier than that are somewhat spotty. The most consistent weather data of any 1-year period in the data set are from August 15, 1987 to August 14, 1988. This time period was selected, and the data were used in these simulations. Where gaps existed (they were only 2 days missing), weather data from the previous day were used to fill in the gaps. The procedures used to estimate missing data are summarized below.

Pressure. The pressure data available in the data set are spotty at best. There are entire months with no pressure data. Therefore, the pressure is assumed to be constant at a value of 81500 Pa, or the approximate value at 1791 m (Wallace and Hobbs, 1977).

Air Temperature. Minimum and maximum air temperature data are available from the weather data files. In order to generate time-dependent temperature data, an expression given by Fayer (2000) has been used that assumes a sinusoidal variation, or

$$T_a(t_d) = T_{mean} + T_{amp} \cos[(\pi/12)(t_d - 15)] \tag{1}$$

where T_{mean} (K) and T_{amp} (K) are the average temperature and the air temperature amplitudes (i.e., the difference between the maximum and minimum temperatures), respectively, and t_d (hr) is time of day. In equation (1), the daily minimum and maximum air temperatures are assumed to occur at 3 am and 3 pm, respectively.

Relative Humidity. Relative humidity information was calculated from vapor pressure information. A daily value of the vapor pressure is given, which is assumed constant for the entire day. The time-dependent relative humidity is calculated from

$$RH(t_d) = 100 \frac{P_v}{P_{sat}(T_a(t_d))} \tag{2}$$

where P_v is the vapor pressure data in the weather files, and P_{sat} is the saturation pressure based on the estimated air temperature data (T_a).

Solar Radiation. Solar radiation data were not included in the weather data files. Solar radiation flux is calculated using expressions given by Campbell (1985) and Fayer (2000), or

$$S_t = S_{ext}\, T_t \sin(e) \tag{3}$$

where S_t (W/m^2) is the solar radiation at the ground surface, S_{ext} (W/m^2) is the solar constant of 1367 W/m^2, and T_t is the transmission coefficient. Sin(e) refers to the sine of the solar elevation angle, or

$$\sin(e) = \sin(\phi)\sin(\delta) + \cos(\phi)\cos(\delta)\cos[(\pi/12)(t_d - t_0)] \tag{4}$$

$$\sin(\delta) = 0.39785\sin[4.869 + 0.0172J + 0.03345\sin(6.224 + 0.0172J)] \tag{5}$$

where J is the day of the year, ϕ is the latitude, δ refers to the solar declination angle, t_d (hr) is the time of day, and t_0 (hr) is the solar noon. The angles are in radians. The latitude of Kabul is 34.52 deg (0.603 radians). Solar noon is assumed to be 12:00 pm.

The transmission coefficient, T_t, is the ratio between measured to potential solar radiation, which is been calculated by the Bristow-Campbell model (Bristow and Campbell, 1984), or

$$T_t = A[1 - \exp(-B\,\Delta T^C)] \tag{6}$$

where A, B, and C are empirical constants and ΔT ($^\circ$C) is the daily range of air temperature (i.e., the difference between maximum and minimum temperatures). Meza and Varas (2000) have evaluated various models for the estimation of solar radiation from air temperature information. They showed that the Bristow and Campbell model performs well. In general, the constants A, B, and C are functions of the climate and vary from location to location. Bristow and Campbell parameters for different locales are given by the RadEst program (Donatelli, 2002). There are no locations in or near Afghanistan with approximately the same climate, elevation, and latitude as Kabul. The parameters for Clayton, New Mexico, US, were used because of similar climate (semi-arid to arid), latitude (36.47 deg for Clayton vs. 34.52 deg) and elevation (1515 m for Clayton vs. 1791 m for Kabul). The values of A, B, and C are 0.76, 0.127, and 2.0, respectively.

Long-wave Radiation. Data for the long-wave radiation (i.e., radiation emittance) of the atmosphere are not available from the weather data. This information has been estimated from air temperature data. Long-wave radiation is calculated as

$$R_{lw} = \varepsilon_a(c)\,\sigma\, T_a^4 \tag{7}$$

where R_{lw} (W/m^2) is the long-wave radiation, ε_a(c) is the atmosphere's emissivity as a function of cloud cover, c, σ is the Stephan-Boltzmann constant (5.67 x 10^{-8} W/m^2-K^4), and T_a (K) is the air temperature in K. The emissivity of the atmosphere including clouds is given by (Monteith and Unsworth, 1990, as discussed by Campbell and Norman, 1998)

$$\varepsilon_a(c) = (1 - 0.84c)\,\varepsilon_{ac} + 0.84c \tag{8}$$

where ε_{ac} is the clear sky emissivity, or

$$\varepsilon_{ac} = 9.2 x 10^{-6} T_a^2 \tag{9}$$

as given by Brutsaert (1984) and Campbell and Norman (1998) where the air temperature is in K.

The cloud cover fraction, c, has been estimated from the solar radiation transmission coefficient, T_t, through the expression (Campbell, 1985)

$$c = 2.33 - 3.33 T_t \tag{10}$$

The cloud cover fraction is constrained to values between 0 and 1.0. Note that, on a clear day (i.e., c=0), T_t~0.7, which is consistent with transmission coefficient value from the Bristow-Campbell model.

Wind Speed. Wind speed information was also not available in the weather data set. Wind speed is an important factor that influences the thickness of the boundary layers, where the thickness of the boundary layers is inversely proportional to the wind speed. If the wind speed increases, the boundary layer thicknesses decrease.

Wind speed has diurnal and seasonal variations in addition to changes due to weather fronts. No models were found to estimate the wind speed from other meteorological parameters. In order to provide a variation of the wind speed, data for the diurnal variation of wind speed at a height of 2 m for Oklahoma City, Oklahoma, were used (Crawford and Hudson, 1973). Oklahoma City, Oklahoma, has a semi-arid climate somewhat similar to Kabul, so the wind speed variations can be expected to be similar. These data were averaged over an entire year. The data show an essentially constant wind speed of 3.5 m/s between 12:00 am until sunrise, which then increases to about 5 m/s during the day. The wind speed decreases around sunset to the previous value of 3.5 m/s. A similar variation is given by Mahrt (1981) for the Wangara Experiment in Wangara, Australia for a 40-day averaging period (Arya, 1988). Because these data are averaged over time periods longer than one day, the daily extremes of wind speed and boundary layer thicknesses are not reflected in the present simulations. The detailed expressions for the wind speed variation are

12:00 am to 6:00 am	3.5 m/s
6:00 am to 11:00 am	linear increase from 3.5 m/s to 5.0 m/s
11:00 am to 4:00 pm	5.0 m/s
4:00 pm to 8:00 pm	linear decrease from 5.0 m/s to 3.5 m/s
8:00 pm to 12:00 am	3.5 m/s

Precipitation. Daily cumulative precipitation values are included in the weather data file. In the absence of additional information, the precipitation rate is assumed to be constant for the entire 24 hour period. The total rainfall for the year is 18.4 cm.

Summary of Weather Data. The final processed weather data are plotted in Figure 3. The data have been reordered to correspond to the time of the year. Therefore, day 1 is January 1 and day 365 is December 31. The annual weather pattern is a relatively wet spring followed by a dry summer and fall. Note that the winter precipitation is probably snow. At present, T2TNT cannot model freezing conditions, so snow is modeled as rain. The minimum air temperature used in the simulations is 12°C in order to prevent surface temperatures below freezing.

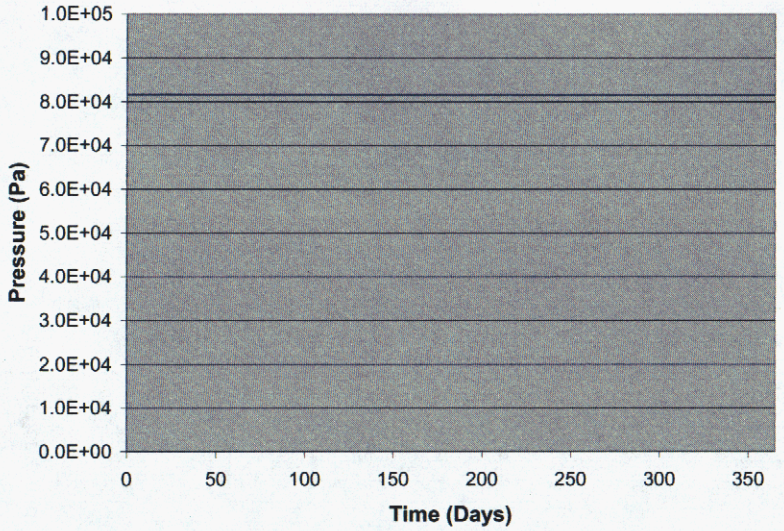
Pressure (Pa)
1.0E+05
9.0E+04
8.0E+04
7.0E+04
6.0E+04
5.0E+04
4.0E+04
3.0E+04
2.0E+04
1.0E+04
0.0E+00
0
50
100
150
200
250
300
350
Time (Days)

(a)

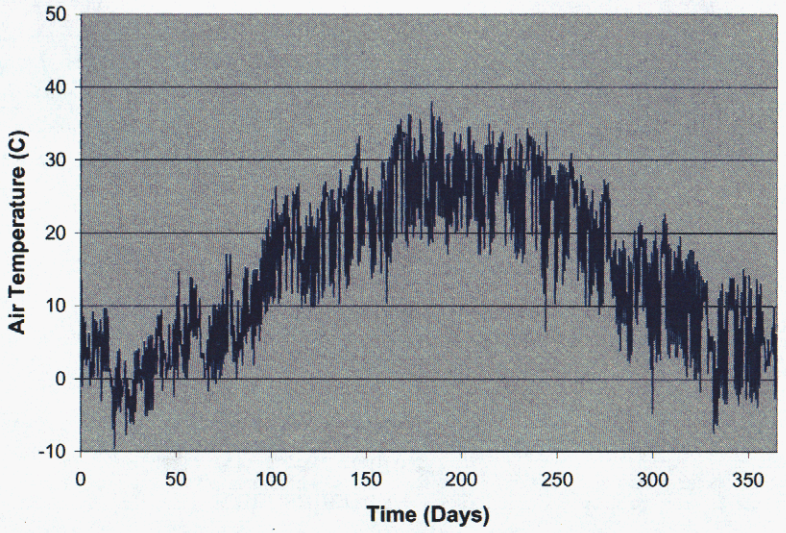
Air Temperature (C)
50
40
30
20
10
0
-10
0
50
100
150
200
250
300
350
Time (Days)

(b)

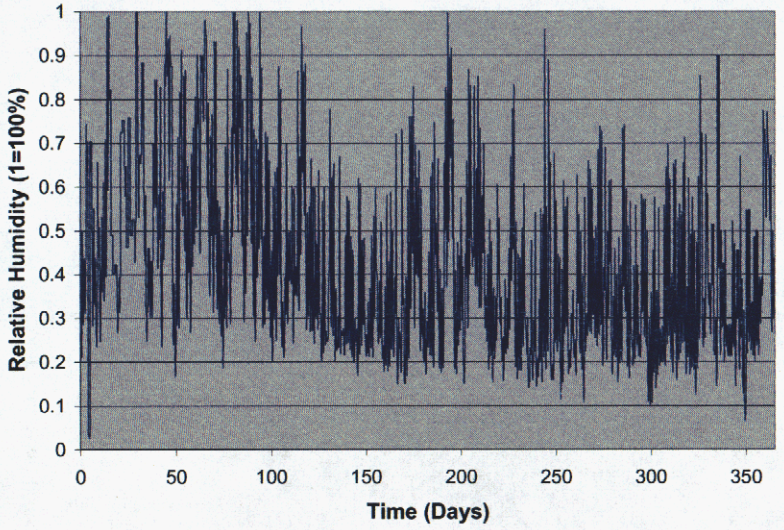
Relative Humidity (1=100%)
1
0.9
0.8
0.7
0.6
0.5
0.4
0.3
0.2
0.1
0
0
50
100
150
200
250
300
350
Time (Days)

(c)

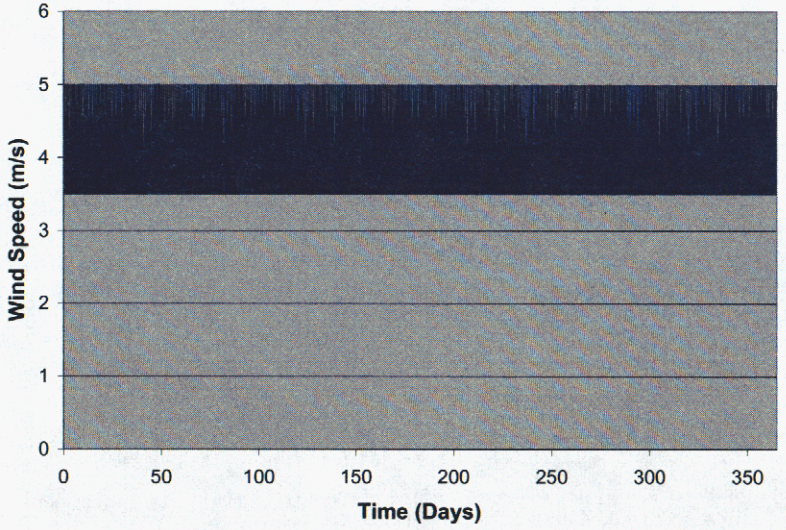
Wind Speed (m/s)
6
5
4
3
2
1
0
0
50
100
150
200
250
300
350
Time (Days)

(d)

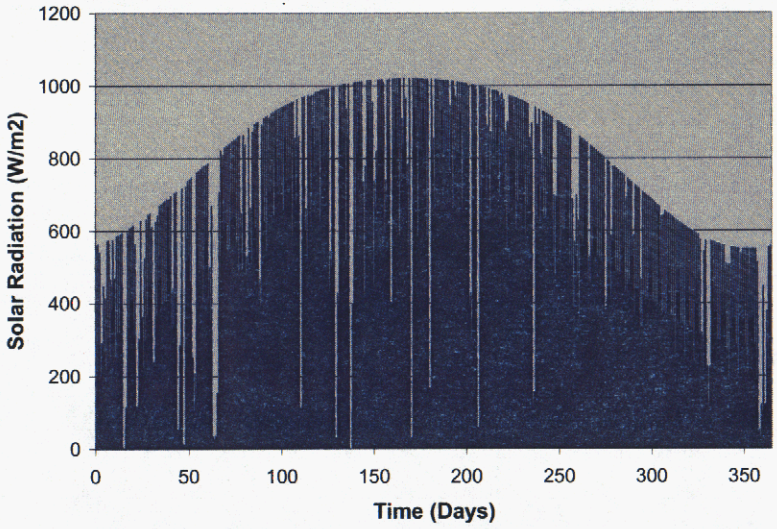

(e)

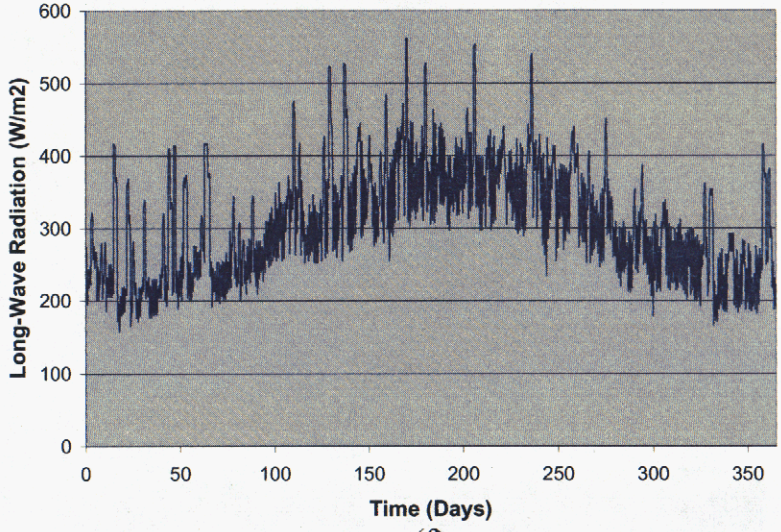

(f)

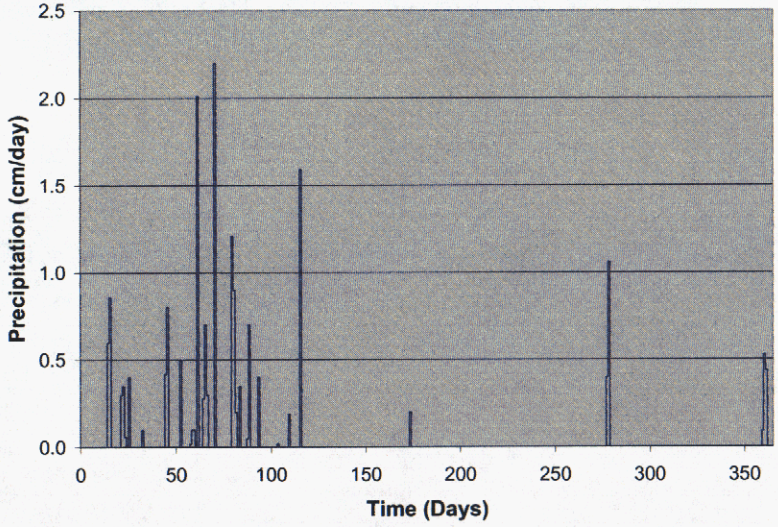

(g)

Figure 3. Final Weather Data
(a) Atmospheric Pressure
(b) Air Temperature
(c) Relative Humidity
(d) Wind Speed (2-m)
(e) Solar Radiation
(f) Long-Wave Radiation
(g) Precipitation

2.2 Boundary Layer Methodology

Boundary layers occur in the atmosphere at the interface with the soil. In the case of the velocity (momentum) boundary layer, the transition is from atmospheric wind speed conditions to zero velocity at the top of the soil. There are different boundary layers for momentum (velocity), energy, and mass transfer. The evaporation boundary layer is a mass transfer boundary layer that is generally a thin (~1-10 cm) layer of air at the surface in which the water vapor concentration changes from the value at the land surface to the value in the atmosphere. Within this water vapor boundary layer is a thinner (~0.25–2.5 cm) chemical boundary layer where the chemical concentration decreases from the value at the soil surface to a value of zero in the atmosphere. The procedure to estimate the boundary layer thickness is adapted from the SiSPAT code (Braud, 1996; Braud et al., 1995) with permission.

For momentum, mass (water vapor), and heat transfer, the turbulent fluxes between the atmosphere and the soil surface are formulated in terms of resistances, or

$$\tau = \rho_a u^{*2} = -\rho_a (U_a - U_{av}) / R_{aM} \quad (11a)$$

$$E = -\rho_a (\omega_a - \omega_{av}) / R_{aV} \quad (11b)$$

$$H = -\rho_a c_p (T_a - T_{av}) / R_{aH} \quad (11c)$$

where τ, E, and H are the momentum, mass (water vapor) and heat flux through the boundary layer, respectively. These formulae are appropriate when plants are included, where the "av" subscript refers to average conditions within the plant canopy, and the transfers are between the atmosphere and the canopy. In the present situation, when there is bare soil, or no plant canopy, the exchanges are between the atmosphere and the ground surface, and the "av" subscript conditions are replaced by the surface conditions.

The momentum equation is needed when a plant canopy is included to estimate the momentum distribution between the atmosphere, plant canopy, and the ground, and to calculate an average velocity in the canopy. For bare soil, the momentum equation is not needed, and a momentum (velocity) boundary layer thickness is not calculated.

Mass transfer (water vapor) and heat transfer boundary layer resistances, R_{aV} and R_{aH}, are calculated as detailed below. The boundary layer thicknesses can then be estimated. The boundary layer resistances are calculated as follows.

Wind speed and temperature profiles above the surface are assumed to be logarithmic according to

$$U_a(z_a) = \frac{u^*}{k}\left(\log\left(\frac{z_a - d}{z_{om}}\right) - \psi_m\left(\frac{z_a - d}{L}\right)\right) \quad (12a)$$

$$T_a(z_a) = \frac{\theta^*}{k}\left(\log\left(\frac{z_a - d}{z_{oh}}\right) - \psi_h\left(\frac{z_a - d}{L}\right)\right) \quad (12b)$$

where u* is the friction velocity, θ* is a characteristic temperature, d is the displacement height, z_{om} is the momentum roughness length, z_a is the elevation of the measured velocity (wind speed) and air temperature (they may be different), k is the von Karmen constant, and z_{oh} is the roughness length for heat. L is the Monin-Obukhov length given by

$$L = \frac{u^{*3}\,\overline{T}}{g\,k\left(-\frac{H}{\rho c_p}\right)} = \frac{u^{*3}\,\overline{T}}{g\,k\,\theta^*} \tag{13}$$

The roughness lengths are related by

$$z_{oh} = z_{om}\exp\left(-\left(2.46\,\mathrm{Re}^{*0.25} - 2\right)\right) \tag{14}$$

$$\mathrm{Re}^* = \frac{u^*\,z_{om}}{\nu} \tag{15}$$

The parameter d is a displacement height that is related to the height of the vegetation, while z_{om} is a roughness length for momentum that generally depends on the local terrain (see Arya, 1988). For bare soil, which is the only condition treated in the present version, d = 0., and z_{om} = 0.005 m.

The functions Ψ_m and Ψ_h in the velocity and temperature profile relationships are stability functions for the atmosphere and are given by

$$\psi_m(y) = 2\log(a) + \log(b) - 2\tan^{-1}(x) + \frac{\pi}{2} \qquad y <= 0 \tag{16}$$

$$\psi_m(y) = -\left[0.7\,y + 0.75\left(y - \frac{5}{0.35}\right)\exp(-0.35\,y) + \frac{3.75}{0.35}\right] \qquad 0 < y <= 1 \tag{17}$$

$$\psi_m(y) = -5\left(1 + \log(y)\right) \qquad y > 1 \tag{18}$$

and

$$\psi_h(y) = 2\log(b) \qquad y <= 0 \tag{19}$$

$$\psi_h(y) = -\left[\left(1 + \frac{2}{3}y\right)^{1.5} + 0.667\left(y - \frac{5}{0.35}\right)\exp(-0.35\,y) + \frac{2.985}{0.35}\right] \qquad 0 < y <= 1 \tag{20}$$

$$\psi_h(y) = -5\left(1 + \log(y)\right) \qquad y > 1 \tag{21}$$

where

$$x = (1 - 16\,y)^{1/4} \tag{22}$$

$$a = \frac{1+x}{2} \tag{23}$$

$$b = \frac{1+x^2}{2} \tag{24}$$

The equations for the logarithmic velocity and temperature profiles and the Monin-Obukhov length, L, are iterated upon to find the appropriate solution for the characteristic velocity, u^*, temperature, θ^*, and L. The resistance to heat is based on a combination of the turbulent flux equation, the temperature profile equation, and the Monin-Obukhov length, or

$$R_{aH} = \frac{\left(\log\left(\frac{z_a - d}{z_{oh}}\right) - \psi_h\left(\frac{z_a - d}{L}\right)\right)}{k\,u^*} \tag{25}$$

and the resistances for heat and mass transfer are assumed to be equal for simplicity, or

$$R_{aV} = R_{aH} \tag{26}$$

The mass transfer (water vapor) and heat transfer boundary layer thicknesses can be estimated from the resistance given above and the diffusion coefficient. For water vapor, the boundary layer thickness is given by

$$\delta_{aV} = R_{aV}\,D_V \tag{27}$$

Note that Jury et al. (1983, 1984) estimated the average evaporation boundary layer thickness using this approach as 0.5 cm.

In reality, the boundary layer thickness estimated from this procedure is only an approximation. Turbulence enhances diffusion in the outer portion of the boundary layer, so the diffusion coefficient and boundary layer thickness given by equation 27 can be thought of as a minimum value. Based on velocity profiles for air flowing over a flat plate (White, 1974), the total boundary layer thickness may be up to a factor of 10 times the value estimated in equation 27. Note that the change in water vapor concentration is not linear in the boundary layer; it changes much more quickly nearer the soil surface than further out in the boundary layer.

The above discussion is for the water vapor mass transfer boundary layer thickness. For diffusion into air, the mass transfer boundary layer thickness for the various components (water vapor, TNT, DNT, and DNB) is proportional to the square root of the diffusivity of the component (Bejan, 1995). The diffusivity of the various landmine chemicals given in Table 1 is about 0.25 that of water vapor (22,500 cm^2/day, Pruess, 1991), so the chemical boundary layer thickness is about 0.5 that of water vapor. In addition, the boundary layer thickness depends on the starting location of the various boundary layers; the boundary layer thickness increases with distance. For water vapor, the starting location may be the edge of the field, while the starting

location for the landmine chemicals is the edge of the chemical plume for a particular mine. The ratio of chemical to water vapor boundary layer thickness due to the different starting locations is assumed to be 0.5 in the present simulations. Combined with the different thickness due to the diffusion coefficient, the chemical to water vapor boundary layer thickness ratio is assumed to be 0.25.

The impact of this thickness due to different starting locations is to decrease the chemical boundary layer resistance to mass transfer into the atmosphere. The impact is probably small because most of the resistance to chemical movement is in the soil, not in the boundary layer. A smaller ratio will also reduce the reported chemical boundary layer thickness.

The reported chemical boundary layer thickness values in this report consider the entire thickness of the boundary layer, which is 10 times the diffusion coefficient value (equation 27), and use the chemical to water vapor thickness ratio of 0.25.

2.3 T2TNT Description

The physical processes modeled by T2TNT include a number of enhancements made since the description by Webb et al. (1999). These enhancements include the mine source rate, which is dependent on the local temperature, and the degradation half-life, which is dependent on the local soil saturation and temperature. The properties used in the simulations are summarized in Table 1. The behavior of TNT and DNT are simulated in the present investigation; DNB is not included because not all of the necessary DNB chemical properties are available.

Sorption. Sorption to soil particles is important in the distribution of landmine chemicals among the gas, liquid, and solid phases, especially for low moisture content conditions (Webb et al., 1999). At low soil liquid saturations, vapor-solid sorption can be significant for explosive compounds (Phelan and Barnett, 2001a). The total effective sorption coefficient, K_E, is a combination of liquid-solid sorption and vapor-solid sorption given by (Shoemaker et al., 1990)

$$K_E = K_d + K_H K_{VS} \tag{28}$$

where

$$K_{VS} = K_d' - K_d / K_H - w_m / K_H \rho_l \tag{29}$$

The expression for vapor-solid sorption, K_{VS}, is from Ong et al. (1991). Note that equation (29) as given in Ong et al. (1991) has an incorrect sign on the last term (confirmed by Lion, personal communication, 1999). In the above equation, w_m is the mass moisture content, or the mass of water per mass of soil. K_{VS} models the distribution of vapors between the solid and gas phases.

Table 1. Estimated Chemical Properties

	2,4,6-TNT	2,4-DNT
K_H (25°C)	8.2E-7	1.0E-5
K_d (mL/g)	0.9	0.5
A_0 ($\log_{10}K_d$'(w=0.))	15.3	13.1
α	51.2	43.5
D_l (cm^2/day)	0.580	0.632
D_g (cm^2/day)	5530.	5790.
Molecular Weight	227.13	182.14
$t_{1/2}$ (days)	Table 2	Table 2

The K_d' model of Petersen et al. (1995) has been used in T2TNT. K_d' as a function of moisture content is given by

$$K_d' = 10^A \tag{30}$$

$$A = (A_0 - \beta)e^{-\alpha w} + \beta \tag{31}$$

where

$$\beta = \log_{10}(K_d/K_H + w_m/K_H\rho_l) \tag{32}$$

$$A_0 = \log_{10}(K_d'(w=0)) \tag{33}$$

K_d' can be thought of as the sorption coefficient based on vapor-solid interactions, while K_d is based on liquid-solid interactions. The variation of K_d' is such that as the exponential term approaches zero, K_d' approaches $K_d/K_H + w_m/K_H\rho_l$, and K_{VS} approaches zero. Under these conditions, the effective sorption coefficient becomes the liquid-solid sorption value, K_d. The parameters for vapor-solid sorption of TNT and DNT on Sandia soil have been measured by Phelan and Barnett (2001a) and are shown in Figure 4. As the soil liquid saturation decreases below 0.30, the value of K_d' increases dramatically due to vapor-solid sorption. This variation is important in understanding some of the numerical results shown later.

The liquid-solid sorption coefficients, K_d, in Table 1 used in the model are 0.9 and 0.5 mL/g for TNT and DNT, respectively (Phelan and Webb, 2002). Based on data-model comparisons (Phelan et al., 2000), the liquid-solid sorption coefficients are saturation weighted, or multiplied by the liquid saturation.

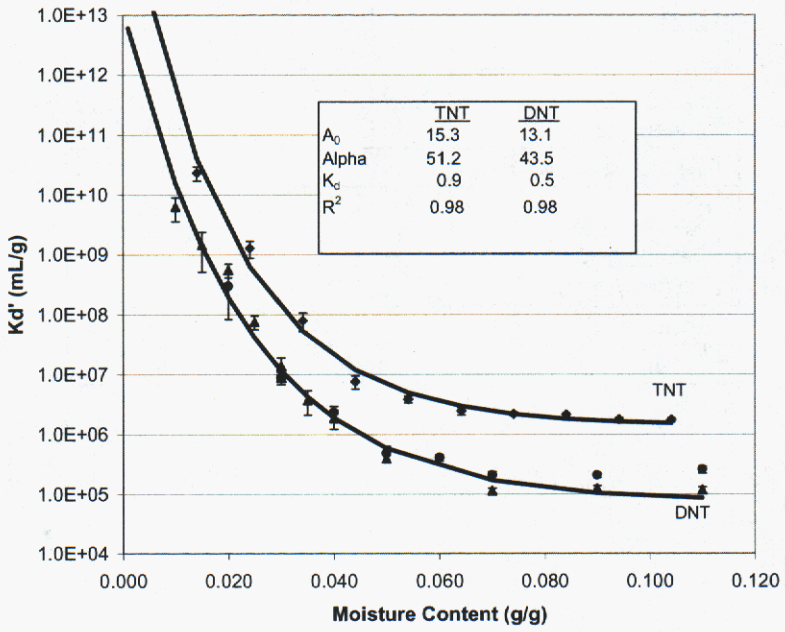

Figure 4. K_d' Variation With Liquid Saturation for TNT and DNT

Chemical Half Life. The half lives for TNT and DNT are based on data summarized by Phelan and Webb (2002). First-order degradation is assumed for simplicity. The values for TNT are highly dependent on the temperature and the soil moisture content as the half-life decreases significantly with increasing temperature and increasing soil moisture content. The values range from a maximum half-life of 1155 days to a minimum value of 1 day. The values used for the TNT half-life in this analysis are summarized in Table 2 below.

Table 2.
TNT Half-Lives

	Temperature (°C)		
Soil Moisture Content (%, w/w)	5	24	40
1	1155	730	140
5	16	1	1
10	6	1	1

Linear interpolation of the values in the table is used to determine the half-life for given conditions. The values are kept constant outside of the range of the table; extrapolation is not used. The values in the table are directly from Phelan and Webb (2002) except for the half-life at 24°C and a moisture content of 10%. Phelan and Webb (2002) had a value of 3 days, while the above table has a 1-day half-life. The revised value is more consistent with the general trend of decreasing or constant half-life with increasing moisture content than the original number. The half-lives for DNT are assumed to be equal to those of TNT because sufficient information is not available to estimate DNT half-lives. However, some data indicate that DNT may have a greater half-life than TNT under equivalent conditions (Phelan and Webb, 2002).

Landmine chemicals may exist as vapors in the gas phase, as dissolved gases (solutes) in the liquid phase, and as sorbed gases and solutes on the solid phase. In the present model, only the mass of the dissolved gas (solutes) undergo degradation.

Source Rate. The chemical source rate from buried landmines is a function of temperature. The temperature dependence of the source rate is modeled as an exponential variation with an exponent of 0.11, or

$$Source\,Rate(T) = Source\,Rate\left(at\,22\,^{\circ}C\right)\exp\left(0.11*\left(T-22\right)\right) \tag{34}$$

where the temperature is in °C (Phelan and Webb, 2002; Leggett et al., 2001).

Other Properties. The values of Henry's constant (K_H) in Table 1 for TNT and DNT are based on vapor pressure data from Pella (1977) and water solubility data from Phelan and Barnett (2001b). The variation in Henry's constant with temperature is included. The diffusion coefficients are from Rosenblatt et al. (1991).

Radiation Balance at Soil Surface. The radiation balance at the soil surface is calculated according to the procedure developed by Braud (1996) for the SiSPAT program (see also Braud et al., 1995), portions of which have been incorporated directly into T2TNT with permission. For the present simple case of a bare soil, the long-wave and solar radiation balances reduce to

$$R_{solar,net} = S_t\left(1-\alpha_{bg}\right) \tag{35}$$

$$R_{lw,net} = \varepsilon_g\left(R_{lw}-\sigma T_{surface}^4\right) \tag{36}$$

where the emissivity, ε_g, and albedo, α_{bg}, of the soil are important parameters. Note that the net long-wave radiation also includes the radiation emitted by the soil surface.

2.4 Simulation Model

The simulations use a one-dimensional uniform soil column with a water table 10 m below the surface. The mesh in the top 35 cm is shown in Figure 5. A capillary fringe forms above the water table. Air and vapor diffusion and advection occur in the unsaturated soil above. Most of the weather conditions (pressure, air temperature, relative humidity, wind speed) are coupled to the soil surface through the water vapor and chemical boundary layers. The boundary layer resistances and thicknesses are based on atmospheric and soil surface conditions as detailed in section 2.2. The rest of the weather factors (solar radiation, long-wave radiation, precipitation) are directly imposed on the soil surface. A PMN landmine buried 5 cm below the surface is included in the problem by adding source terms of TNT and DNT. Because the PMN mine has a rubber top, the source is assumed to emanate from the top of the mine. The physical presence of the mine cannot be included due to the one-dimensional nature of the model.

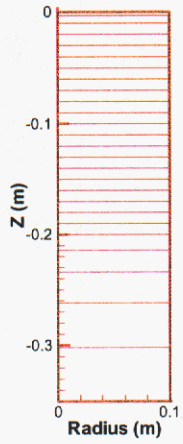

Figure 5.
Near Surface Mesh

The simulations were run in three phases. The first phase is the initiation phase, which uses "average" yearly data for a total simulation time of 100 years in order to condition the 10-m deep soil environment prior to burial of the landmine. The second phase consists of three one-year simulations using the actual weather data and initial conditions from the end of the 100-year initialization phase. This second phase conditions the top 1 m or so with actual weather conditions. The third phase adds the landmine source with the weather data again and the initial conditions from the second phase simulations. The initial conditions for this third phase are much more realistic than those used for the second phase because they are calculated based on three years of actual weather data rather than average conditions. The landmine is planted on June 15. Chemical movement calculations continue for 2 ½ years after the landmine is placed in the ground

Mine Flux Data. The source rate for the PMN mine is 70 and 10 µg/mine/day for TNT and DNT, respectively at 30°C, from data in Phelan et al. (2002). The source rate changes exponentially with temperature as discussed in the previous section. The source rate values corrected back to 22°C are 29 and 4 µg/mine/day for TNT and DNT, respectively.

Soil Parameters. The soil parameters used in the simulation are summarized in Table 3. These parameters are from the tabulation of Carsel and Parrish (1988) for a typical sandy soil. The two-phase characteristic curves are from van Genuchten (1980), or

$$P_c = -\frac{1}{\alpha_{vG}}\left(S_e^{-1/m} - 1\right)^{(1-m)} \tag{37}$$

and

$$k_{r,l} = S_e^{1/2}\left(1 - \left(1 - S_e^{1/m}\right)^m\right)^2 \tag{38}$$

Table 3.
Soil Parameters

Permeability	8.4×10^{-12} m
Porosity	0.43
Fully-Saturated Conditions[a] (S_S)	0.999
Liquid Residual Saturation ($S_{l,r}$)	0.1046
Matching Saturation (S_l^* - see Webb, 2000)	0.1105
Air Entry Pressure Parameter ($1/\alpha_{vG}$)	676. Pa
n	2.68
m (= 1 – 1/n)	0.627
Wet Thermal Conductivity (deMarsily, 1986)	3.0 W/m-K
Dry Thermal Conductivity (deMarsily, 1986)	0.6 W/m-K
Volumetric Heat Capacity (de Marsily, 1986)	1.9×10^6 J/m^3-K
Albedo of Soil (Arya, 1988)	0.40
Emissivity of Soil (Arya, 1988)	0.87

[a] - assumed

$$S_e = \frac{S - S_{l,r}}{S_s - S_{l,r}} \tag{39}$$

where the capillary pressure, P_c, is the difference between the liquid pressure and the gas pressure, or $P_l - P_g$, which is negative.

Vapor pressure lowering due to the capillary pressure and implied air-liquid interface curvature has been included. Vapor pressure lowering is due to the curvature of the gas-liquid interface and can be related to the capillary pressure (Dullien, 1992). This relationship is often represented by Kelvin's equation (Edlefsen and Anderson, 1943, as given by Pruess, 1991), or

$$P_v(T, S_l) = f_{VPL}\, P_{sat}(T) \tag{40}$$

where

$$f_{VPL} = \exp\left\{\frac{m_l\, P_c(S_l)}{\rho_l\, R\, T}\right\} \tag{41}$$

and the terms are defined in the Nomenclature section.

There is some concern about the applicability of the capillary pressure relationship given by equation 37 at very high capillary pressures. Specifically, the capillary pressure approaches infinity as the liquid saturation approaches liquid residual saturation; below liquid residual saturation, the capillary pressure is undefined. These concerns have been addressed by an

extension of two-phase capillary pressure curves into the dry region as developed by Webb (2000). In this model, the resulting capillary pressure is continuous and finite in the entire liquid saturation region down to zero liquid saturation.

The dry and wet thermal conductivities of the soil are based on the mean of the range for sand and are 0.6 and 3.0 W/m-K, respectively (deMarsily, 1986). The volumetric heat capacity for sand is 1.9×10^6 J/m^3-K (deMarsily, 1986). The emissivity, ε_g, and albedo, α_{bg}, of the soil has been estimated as 0.87 and 0.40, respectively, based on dry bare sand (Arya, 1988).

Runoff has been included in the model by specifying a maximum value of the soil surface saturation as 0.98. This limit was not reached during these simulations.

3.0 Model Results

3.1 Gas-Phase Concentrations

3.1.1 Yearly Variation

The gas-phase concentration of TNT at the surface is shown in Figure 6a for the year of landmine burial, which occurred on June 15 (Day 166 on the Time scale). The chemical signature reaches 10^{-12} ng/L, or 1 molecule per 100 mL of air (approximately one large sniff by a dog), (Phelan and Webb, 2002), about 8 days after burial. This value is considered to be the lower limit of detection by dogs. The TNT concentration continues to increase during the first year with local spikes in the concentrations caused by weather events, primarily precipitation. The TNT gas-phase concentrations at the surface for years 2 and 3 are shown in Figures 6b and 6c. In years 2 and 3, the concentrations are very similar, with only about a factor of 3 or less difference for the same time of year. This trend indicates that the transient time for landmine chemical movement is about 6 months. After that, the concentrations are essentially at steady-state conditions and are not a function of time after landmine burial. Figures 7a through 7c show the same plots for DNT. Based on these results, the seasonal and diurnal effects will be referenced to year 3 of the simulations as the concentrations are not affected by the time of landmine burial but only by weather conditions.

The TNT and DNT surface gas-phase concentrations are very similar. The values are generally within a factor of 2 of each other. The reason for the sharp increases in gas-phase concentrations seen in these figures is that the TNT or DNT sorbed onto the soil particles is released due to the increase in surface soil saturation. This release is due to a decrease in vapor-solid sorption. Previously, Figure 4 showed the impact of soil moisture on vapor-solid sorption. As the soil saturation increases, the sorption coefficient decreases, and the chemical concentration in the gas phase increases. The correlation with surface soil saturation is shown in Figure 8 for TNT. The top curve is the surface gas-phase concentration, while the bottom curve is the surface soil saturation. Every time the surface soil saturation shows a significant increase, the gas-phase surface concentration also increases.

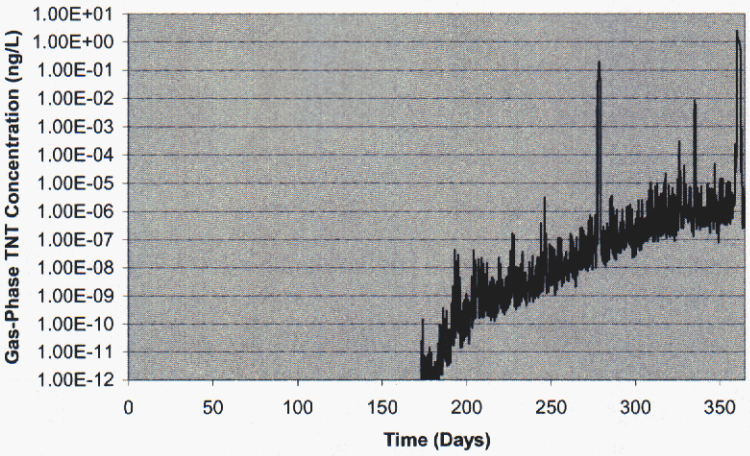

(a) 0 to 1 years

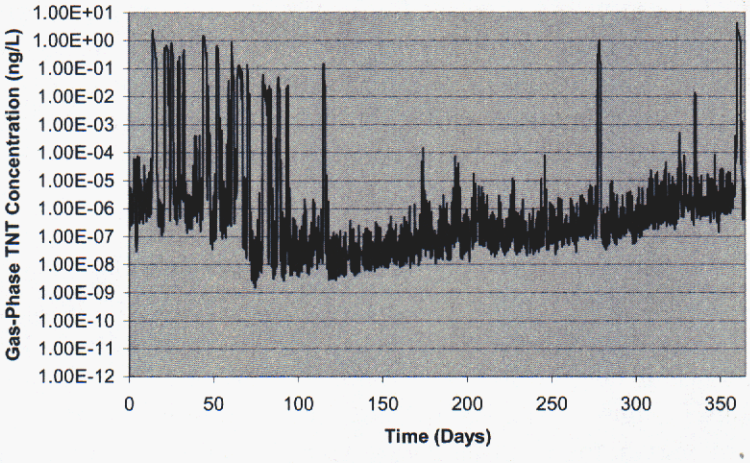

(b) 1 to 2 years

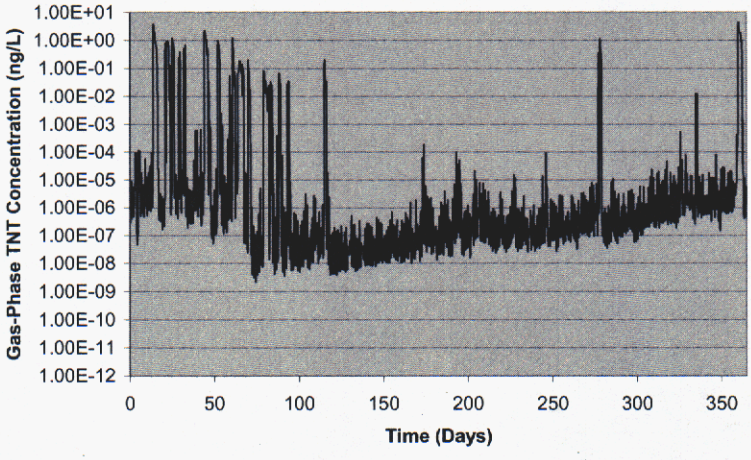

(c) 2 to 3 years

Figure 6.
Surface Gas-Phase TNT Concentration for 0 to 3 Years

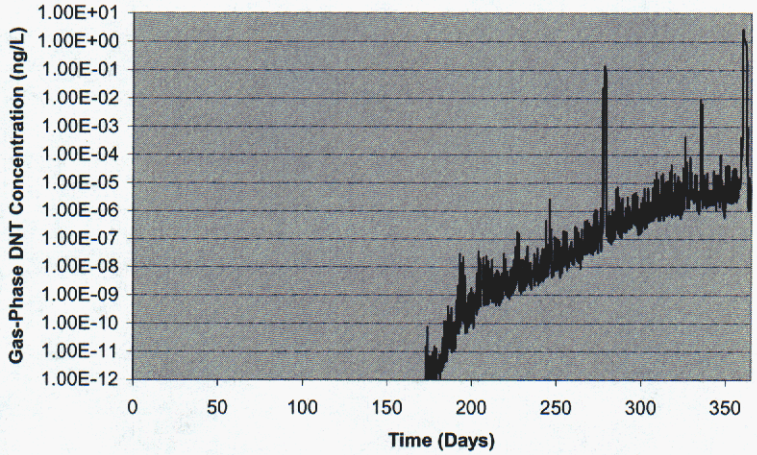

(a) 0 to 1 year

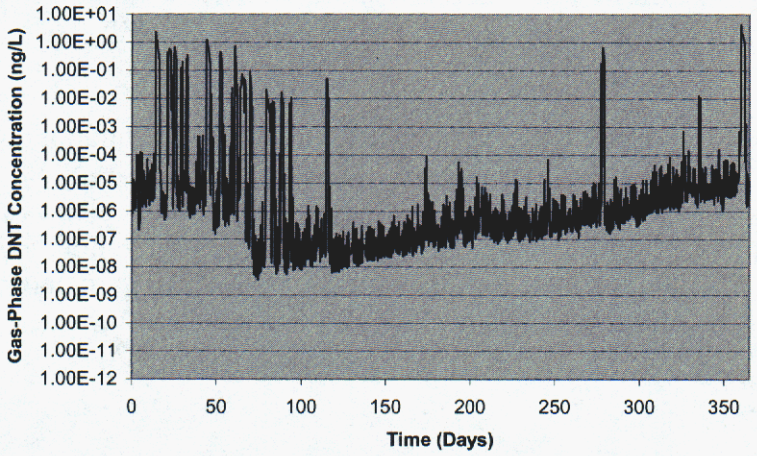

(b) 1 to 2 years

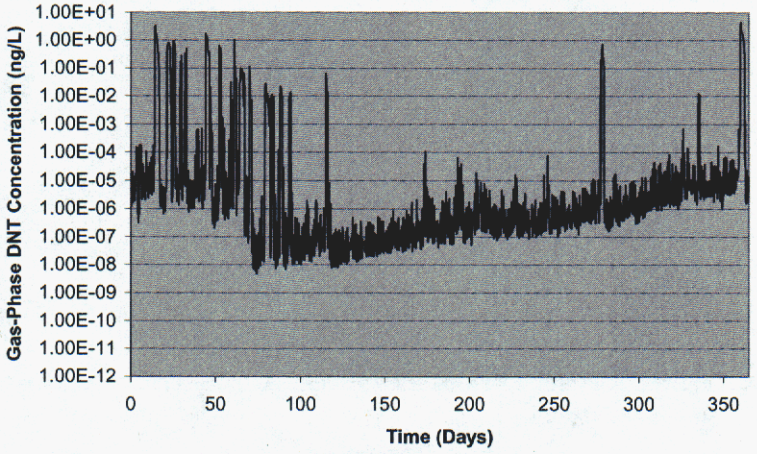

(c) 2 to 3 years

Figure 7.
Surface Gas-Phase DNT Concentration for 0 to 3 Years

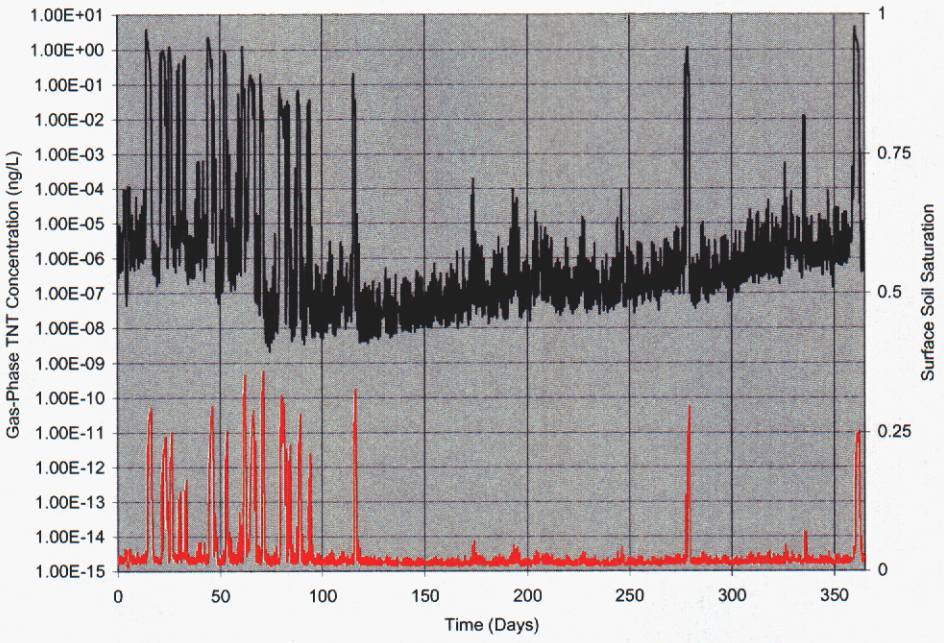

Figure 8.
TNT Surface Gas-Phase Concentration and Surface Soil Saturation for Year 3

The large increases in surface soil saturation are caused by precipitation as shown in Figure 9. The top line is precipitation, while the bottom line is surface soil saturation. Every time rainfall occurs, the surface soil saturation increases dramatically. The small variations in the surface soil saturation are caused by variations in relative humidity and are discussed later under diurnal effects.

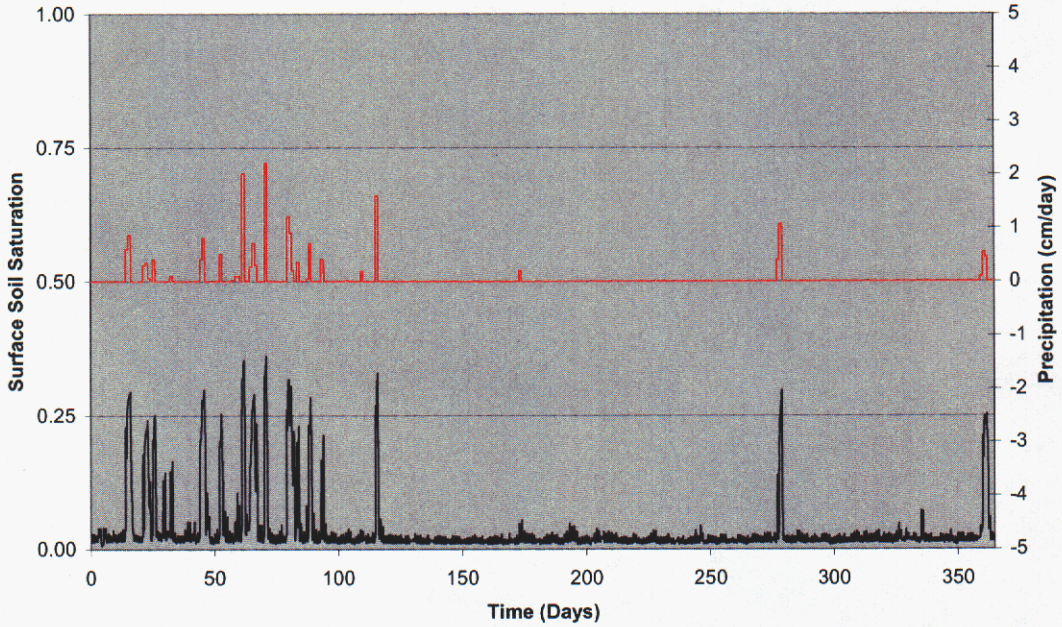

Figure 9.
Surface Soil Saturation and Precipitation for Year 3

The saturation change at the soil surface is confined to the top cm or so of soil. The saturation change at the top of the landmine is shown in Figure 10. The top line is the soil saturation at the top of the landmine, while the bottom line is precipitation. The only significant saturation changes at the top of the landmine are due to the larger precipitation events. The diurnal effects at the top of the landmine are minimal because changes in atmospheric humidity do not affect soil moisture at the depth of the landmine (5 cm).

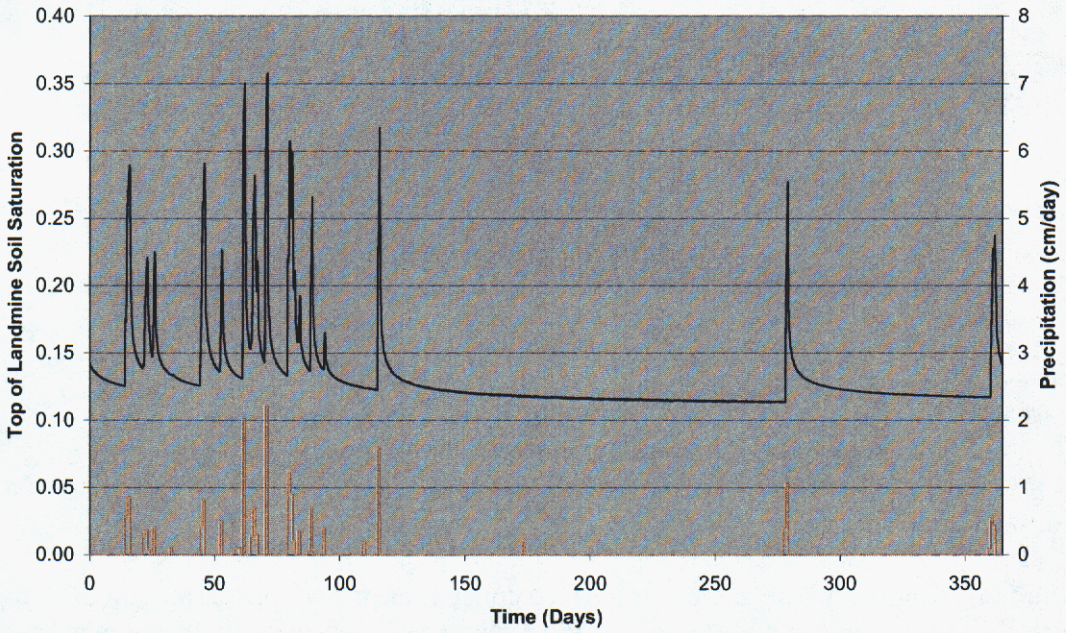

Figure 10.
Soil Saturation at the Top of the Landmine and Precipitation for Year 3

The surface gas-phase concentrations in Figure 6 and 7 show a slight seasonal variation. The values are about a factor of 10 to 100 lower during the summer than during the winter. Part of the reason is the decrease in the chemical half-life with increasing temperature. This decrease in half-life at high temperatures, which is up to 3 orders of magnitude, is partially offset by the increase in the landmine emission rate as the temperature increases. The variation in landmine emission rate as a function of time is given in Figure 11 for TNT, which shows a significant increase in emission rate of about 2 orders of magnitude during the summer compared to winter conditions. The DNT source rate variation would be the same as TNT except with a constant multiplier of 1/7.

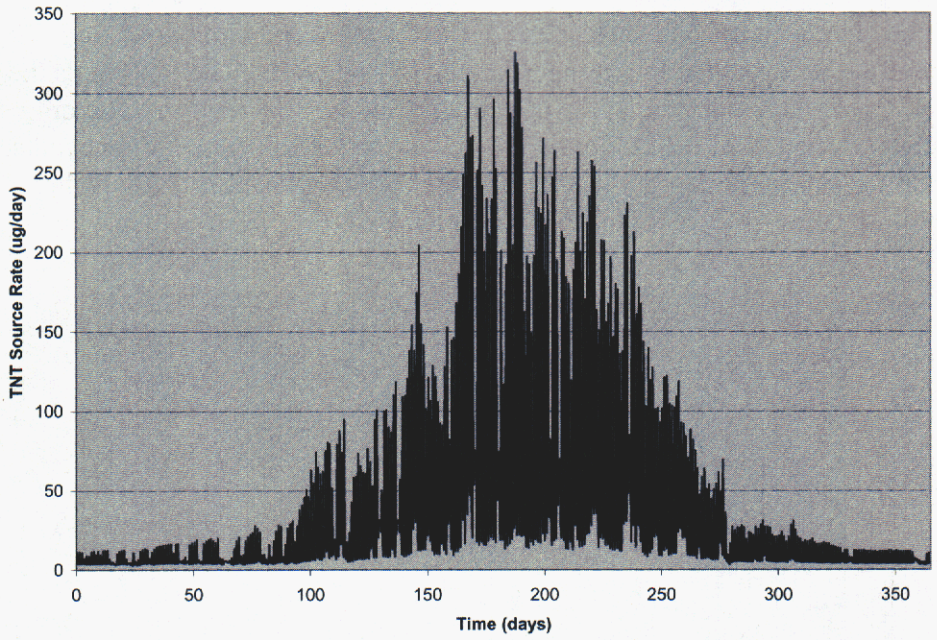

Figure 11.
TNT Landmine Source Rate for Year 3

3.1.2 Diurnal Variation

The diurnal variations in the gas-phase surface concentrations are primarily due to changes in the surface soil saturation. In addition to rainfall, changes in surface soil saturation are caused by diurnal variations in atmospheric relative humidity. Figure 12 shows the time period from 185 to 195 days, which is in early July. The TNT gas-phase concentrations follow the surface saturation. The TNT gas-phase concentration (and surface soil saturation) is a maximum around midnight or slightly later, decreases through the late morning to a minimum value around 12 pm, and then increases during the afternoon and into the evening. This change in surface saturation is driven by the local air temperature variation, solar radiation, and relative humidity changes during the day. The increase in values from the period from 185-190 days to 190-195 days is due to an increase in the relative humidity as indicated in Figure 13.

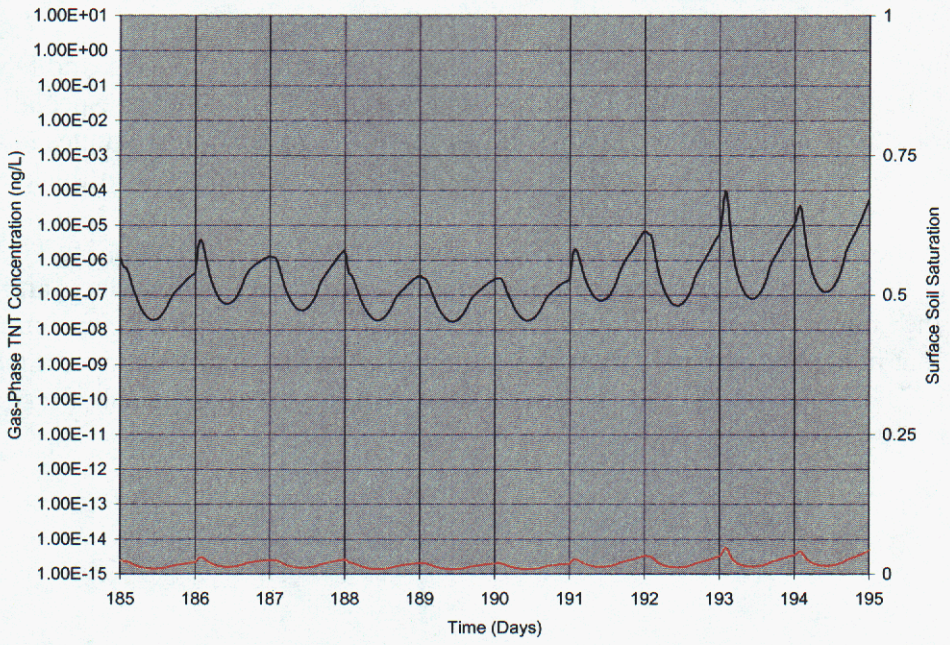

Figure 12.
Surface Gas-Phase TNT Concentration and Soil Surface Saturation for 185-195 Days

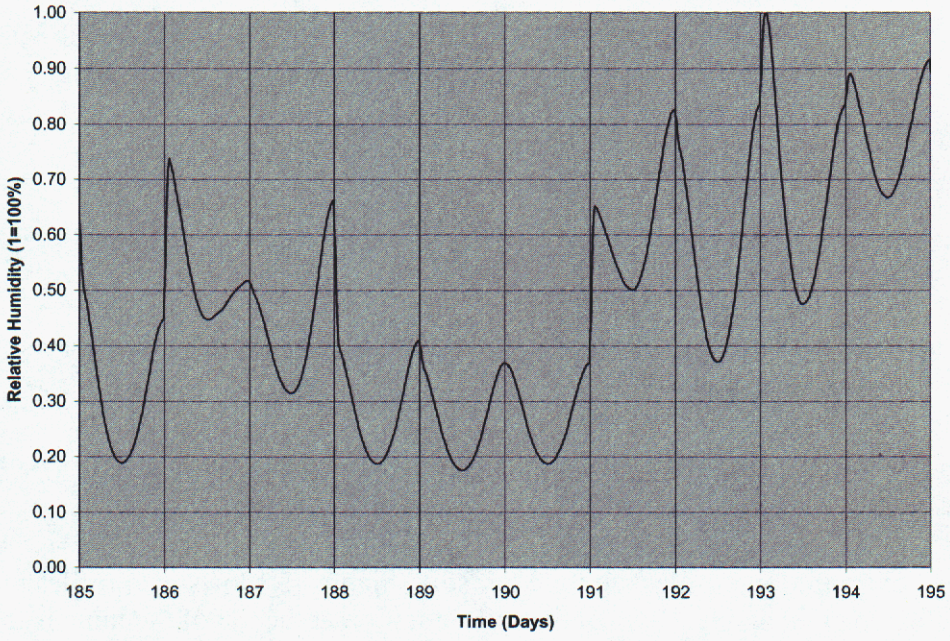

Figure 13.
Atmospheric Relative Humidity for 185-195 Days

3.1.3 Chemical Concentration Profiles

The previous results have only shown the gas-phase concentrations of TNT and DNT at the soil surface. The variation of chemical concentration with depth is dramatic, especially under the dry surface conditions influenced by vapor-solid sorption. The variation continues in the air boundary layer, as the concentration goes to zero outside of the boundary layer thickness.

Results are shown in Figure 14 for Day 202 at about 10:20 pm. The gas-phase TNT and DNT concentrations drop many orders of magnitude as one approaches the soil surface, and it goes to zero outside the boundary layer. The difference between the TNT and DNT concentrations is small. Note that in the present simulation, the estimated chemical boundary layer thickness is only 0.75 cm. The concentration follows the variation in soil saturation, which is a strong function of depth.

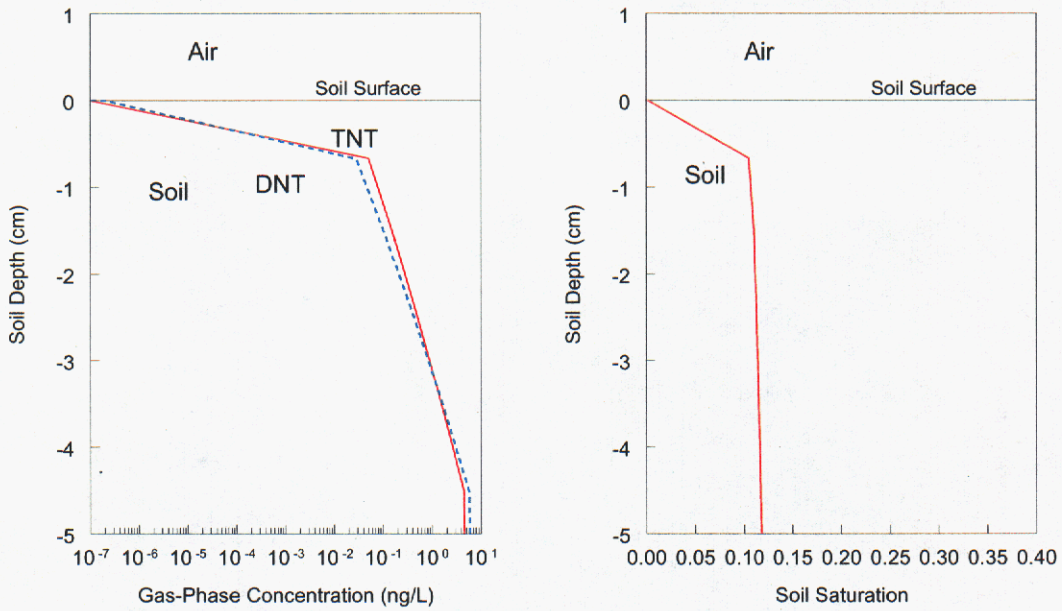

Figure 14.
Dry Soil Gas-Phase Concentration and Saturation Profiles for Day 202

The above concentration profiles are for a dry soil. Figure 15 shows the profiles under wet conditions following rain at day 71 when the soil saturation at the top of the mine is the greatest. The gas-phase concentrations of TNT and DNT are much higher than for the dry conditions at the surface and are relatively constant with depth.

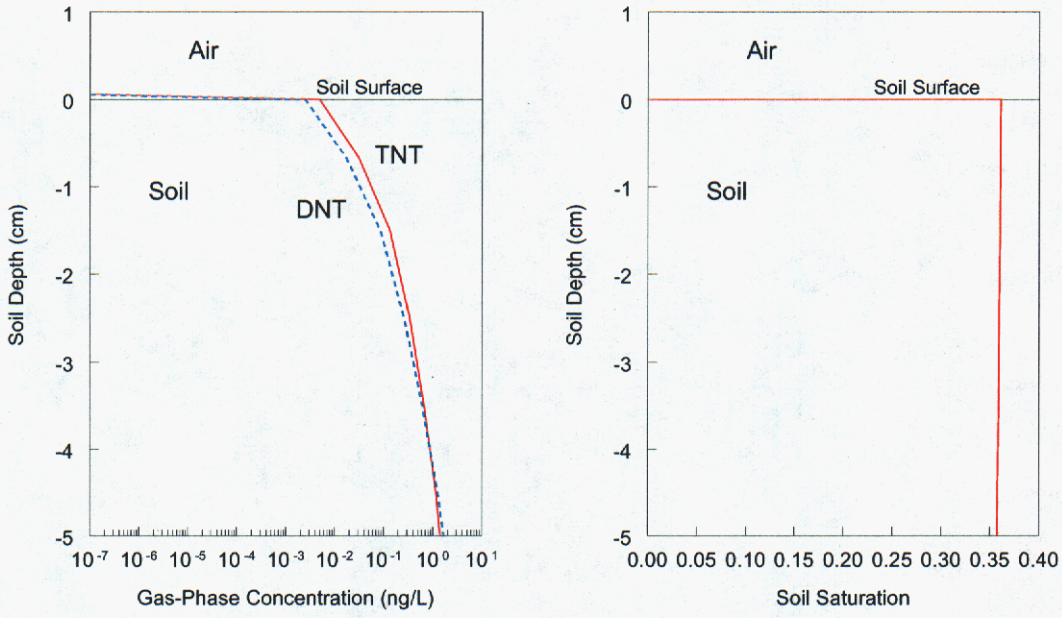

Figure 15.
Wet Soil Gas-Phase Concentration and Saturation Profiles for Day 71

3.2 Soil Concentrations

All the previous results are for gas-phase concentrations as they are thought to be the most important for vapor detection by dogs. In this section, the total chemical mass on the soil will be presented such as would be measured from soil samples around the landmine or on soil particles inhaled by dogs.

3.2.1 Yearly Variation

Figure 16 and 17 show the variation in the concentration on the solid phase at the soil surface during the year for TNT and DNT, respectively. The solid-phase concentrations show much less variation than the gas-phase values. The reason is that while vapor-solid sorption dramatically affects the chemical mass in the gas phase, the amount in the gas phase is a small fraction of that sorbed onto the solid phase, so the net effect is small. In fact the influence of precipitation is generally to decrease the total concentration as opposed to an increase in gas-phase concentration. Much of the total mass on the soil particles is washed down from the surface due to rainfall. As time goes on, the surface total concentration values increase until the next rainfall event.

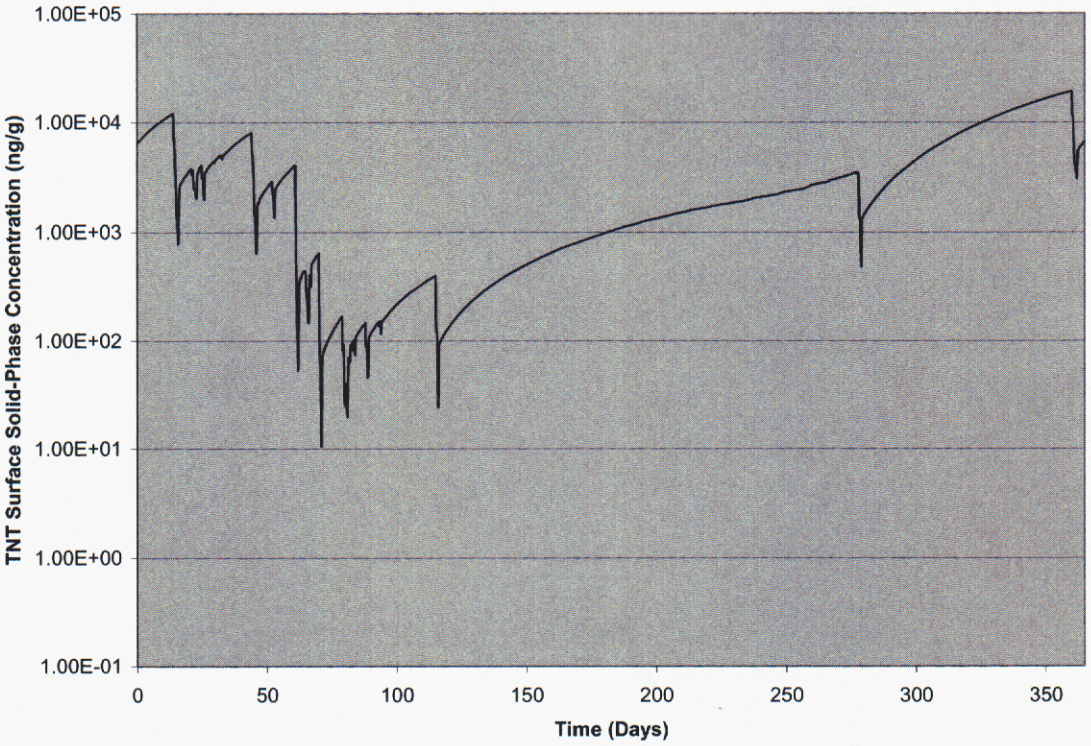

Figure 16.
Surface Solid-Phase TNT Mass Fraction For Year 3

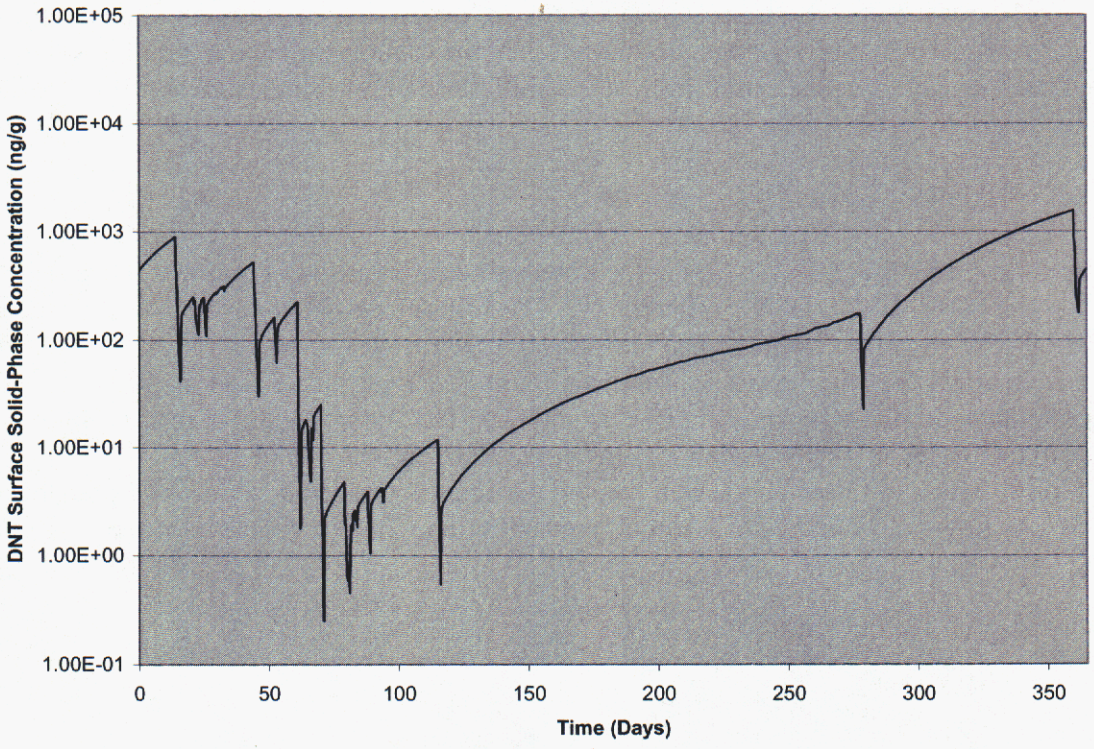

Figure 17.
Surface Solid-Phase DNT Mass Fraction for Year 3

3.2.2 Chemical Concentration Profiles

Figures 18 and 19 show the solid mass fraction of TNT and DNT as a function of depth for dry and wet conditions, respectively, for the same conditions of Figures 14 and 15. The solid mass fraction does not vary significantly with depth in contrast to the gas-phase concentration. In the wet profile, the effect of precipitation washing down the chemical is clearly shown.

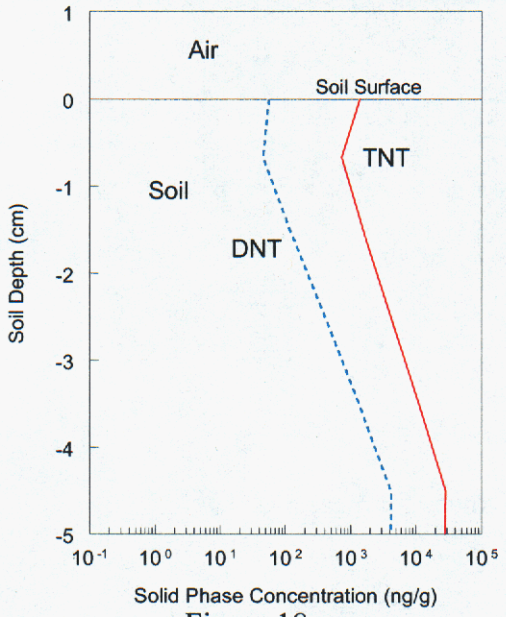

Figure 18.
Dry Soil Profiles for Day 202

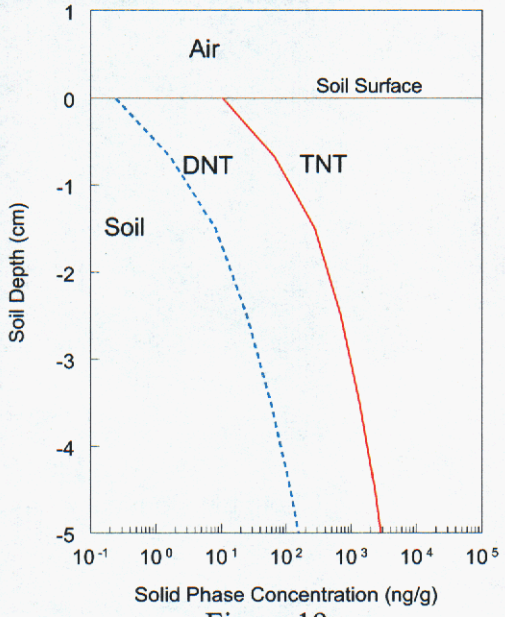

Figure 19.
Wet Soil Profiles for Day 71

3.3 Chemical Boundary Layer Thickness

Figures 20 and 21 show the variation in the chemical boundary layer thickness. Figure 20 gives the yearly variation, which is between 0.5 and 0.9 cm. The range in the chemical boundary layer thickness is small. Figure 20 shows details for the time period 185 to 195 days; the top curve is the chemical boundary layer thickness, while the bottom curve is the wind speed. The boundary layer thickness is inversely proportional to the wind speed. As the wind speed increases, the boundary layer thickness decreases. Due to the lack of wind speed information as discussed in section 2., and the resulting limited range of assumed wind speeds, the boundary layer thickness variation is probably much greater than given in Figures 20 and 21.

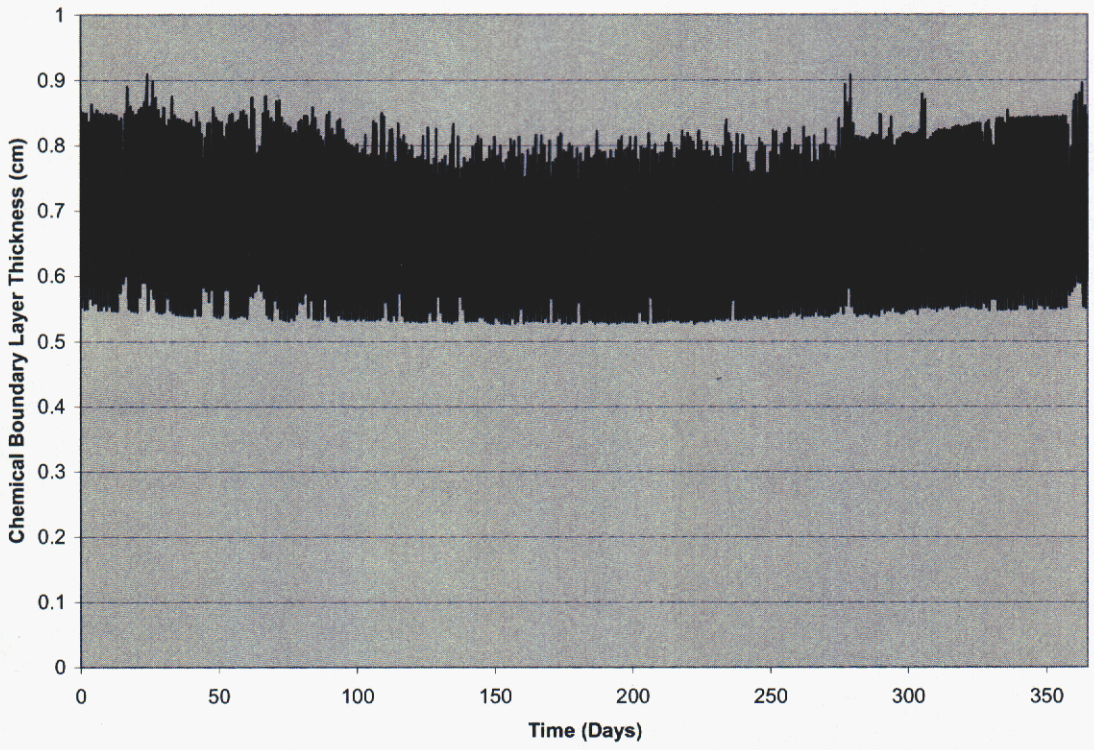

Figure 20.
Chemical Boundary Layer Thickness for Year 3

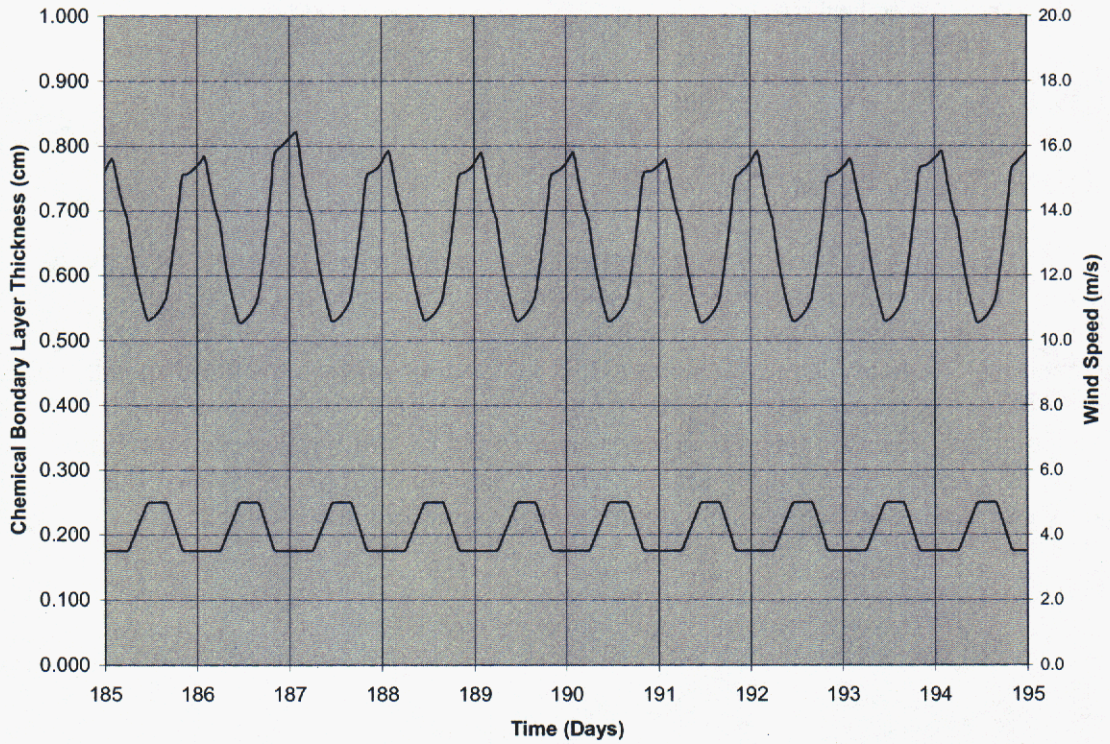

Figure 21.
Chemical Boundary Layer Thickness and Wind Speed for 185-195 Days

4.0 Discussion

Simulation results using T2TNT have been presented for the chemical landmine signature from a PMN landmine for Kabul, Afghanistan. The results indicate that a minimum detectable surface gas concentration of 1 molecule per 100 mL of air occurs about 8 days after the mine is buried, and that the time to steady-state chemical surface gas concentrations is approximately 6 months.

The variation in TNT and DNT surface gas concentrations is driven by changes in the surface soil saturation. Following rainfall, the gas surface concentrations increase dramatically. The surface gas concentrations show a seasonal variation, being lower in the summer than in the winter. While the source rate is much higher in the summer, the much shorter half-lives probably more than offset the increase in source rate.

The diurnal variation of surface gas concentrations is driven by the change in relative humidity. The highest gas concentrations are in the early morning (~3 am), while the minimum values are around noon. This diurnal variation is slightly different than for Ft. Leonard Wood (Webb and Phelan, 2000), where the maximum was at about 7-8 am, or just before sunrise. The minimum value was at noon and in the early afternoon. The differences are probably due to the wind speed and atmospheric relative humidity (RH) information used in each simulation. The present simulations used estimated functions, while the Ft. Leonard Wood results used actual data. These results confirm the importance of wind speed and atmospheric RH data for improved understanding of optimal time of day for mine dog detection work.

The variation in gas concentration with depth is dramatic for dry surface conditions. The gas concentration increases orders of magnitude with depth in the first cm of soil beneath the surface due to decreased vapor-solid sorption. For wet conditions, the increase is much smaller.

The TNT and DNT surface soil concentration on the solid phase has much less variability than the gas concentration. During the year, the values only vary three orders of magnitude. The surface soil concentration decreases significantly following rain. The value recovers until the next rainfall event. The calculated variation with depth is also much smaller than the gas concentration under dry soil conditions; the variability is similar for wet soil.

The chemical boundary layer thickness varies between 0.5 and 0.9 cm. The limited range is due to the wind speed function employed in these simulations. It is expected that the actual range of boundary layer thicknesses will be much greater than given above. Even so, the chemical boundary layer thickness is very small. Any chemical sensing technique (sensors or dogs) needs to be very close to the ground to detect the chemical signature. Accurate wind speed information is essential in the prediction of the boundary layer thicknesses.

In the present report, T2TNT has been used with weather data for Kabul, Afghanistan to predict the chemical concentrations from buried landmines. These results are different from the previous results of Webb and Phelan (2000) for Ft. Leonard Wood in a number of ways.

1. Weather Data. At Ft. Leonard Wood, weather data were obtained from a dedicated weather station for the facility; the only data that had to be estimated was long-wave radiation. In Afghanistan, weather data had to be gleaned from existing weather stations. Unfortunately, because of the conflicts in Afghanistan over the last decade or more, weather station data are sparse and do not include all the required parameters. Therefore, many parameters had to be estimated. The wind speed estimation procedure is particularly simplified. Due to the importance of wind speed on the boundary layer thicknesses, wind speed data are essential for more accurate estimates of surface gas-phase chemical concentrations.

2. Source Rate. The source rate used for Ft. Leonard Wood calculations was for a TMA5 mine (Leggett et al., 2001), and the simulations were run to estimate the steady-state soil concentrations with diurnal and seasonal variations. The source rate was constant in time. For the Afghanistan simulations, the source rate used is for a PMN mine. The temperature dependence of the mine source rate is included in these simulations. In addition, the transient increase in surface soil concentrations is estimated for an assumed mine placement date of June 15.

3. Half-Life. The Ft. Leonard Wood predictions used a constant half-life for the various chemicals. Phelan and Webb (2002) indicate that the half-life is a strong function of soil temperature and moisture content. This variation is included in the present simulations.

4. Cloud Cover. The Ft. Leonard Wood simulations assumed a constant cloud cover fraction of 0.5 in the calculation of long-wave radiation. In the present study, the cloud cover has been estimated from the solar radiation transmission coefficient.

The present simulations have a number of shortcomings. The present simulations are one-dimensional and cannot explicitly include the influence of the mine. The possibility of two-dimensional simulations with weather boundary conditions is currently being investigated. The effect of plants is not included. It is not clear what the net effect of plants would be on the results. The methodology for including plants is part of the SiSPAT program, parts of which have been incorporated into T2TNT with permission. In addition, T2TNT does not allow for freezing temperatures, so a minimum air temperature of 12°C was used. Again, it is not known how this restriction will affect the results.

5.0 Summary

Analysis of the movement of landmine signature chemicals was completed using the simulation model T2TNT for conditions typical of landmines and weather found in Kabul, Afghanistan. Improvements in the simulation model included: 1) TNT and DNT degradation rates as a function of soil moisture content (saturation) and temperature, and 2) actual PMN landmine chemical emission rates as a function of temperature. Variable degradation is important because it virtually ceases at low moisture contents (<1%) and is exceptionally fast at high moisture contents (half-life ~ 1 day). Actual PMN mine flux data that scales with soil temperature improves analysis of diurnal and seasonal effects due to temperature changes just below the ground surface. Both are important changes that improve the reality of the simulations.

Unfortunately, the weather data available for Kabul did not contain sufficient information for a complete analysis of the effects of weather, especially with respect to wind speed and atmospheric relative humidity. Wind speed is a dominant factor in the boundary layer thickness that affects the gas-phase chemical concentration at the soil surface. The wind speed function used in this analysis does not include any low wind speed conditions, where the boundary layer thickness would increase substantially. Thus, the boundary layer estimates shown herein represent smaller values than might actually be found in the field during low wind speed conditions.

The present boundary layer thicknesses are based on steady-state boundary layer modeling. Above the calculated chemical boundary layer thickness, the chemical concentration is zero. Based on this model, sensors (including dogs) must sample from within this boundary layer in order to detect the chemicals. However, during unstable conditions, local thermals may transport significant chemical concentrations into the atmosphere at much greater distances than the calculated boundary layer thickness. These conditions can be evaluated using sophisticated, computationally intensive computational fluid dynamics approaches.

The impact of precipitation on soil moisture content and the gas-phase concentrations of TNT and DNT in the boundary layer continue to dominate the environmental factors analysis. Dramatic increases in gas-phase concentrations occur during precipitation due to the dramatic decrease in vapor-solid sorption as the soil moisture saturation increases. Small increases in gas-phase concentrations also occur during diurnal changes in atmospheric relative humidity. With the limited atmospheric humidity data (daily water vapor pressure values), the diurnal timing of the peak gas-phase TNT or DNT levels is uncertain. This analysis shows peak values in the early morning (0300 hrs), lowest values at mid-day (1200 hrs), then rising again in the afternoon hours. This contrasts the previous Ft. Leonard Wood site analysis where the lowest values were at mid-afternoon and not rising until later in the evening.

The question of how much time is needed for landmine odors to reach the soil surface was partially explored. It appeared that detectable amounts (at least one molecule per dog sniff) occurred within days after a landmine is placed. These values continued to increase and reach near steady-state conditions after about 6 months. These results support field experience that test mines are detectable by dogs within weeks after burial. Much more analysis is needed to explore other mine leakage rates, burial depths, and soil properties.

Seasonal affects show that the gas-phase concentration at the soil surface is lower in the summer by about a factor of 10 to 100 compared to winter conditions. While the landmine release rate is higher during the summer, the increase in degradation rate more than compensates for the source rate increase. Since the degradation rates are only generally understood and not well defined, differences of a factor of 10 to 100 may be not that significant.

The simulation model can also estimate soil residue values. Variation in the surface soil residues may be important if detection also includes inhalation of soil particles. The total solid phase concentration shows a significantly smaller variation than the gas-phase concentrations. In contrast to gas-phase values, precipitation reduces the total concentrations as soil residues are displaced from the surface to soils deeper in the profile. After the rainfall event, the soil residues slowly increase, taking many days to return to pre-rainfall values. If dogs inhale solid particles, the time of day and year should make little difference, and detection after rainfall should be more difficult than before a rainfall. Based on anecdotal evidence, this behavior does not seem to be the case, so vapor phase detection may be the primary sensing method.

Simulation modeling exercises that explore the effects of key factors in the context of the relevant processes and interdependencies is a systems analysis challenge. However, modern computational tools and systems analysis methods now provide this capability. In this effort, a process improved version of the T2TNT code was used to evaluate a single landmine with weather conditions typical of Kabul, Afghanistan.

This analysis showed that estimated vapor concentrations were well within the detectable range for trained mine detection dogs. Seasonal affects were not dominant, indicating that mine detection may be possible year round. However, weaknesses in the weather data add uncertainties in direct application to specific field situations ongoing in Afghanistan today. Improvements in the soil model (e.g. add sub-freezing conditions and plants) are needed. In addition, more advanced computational fluid dynamic model components are needed to better mimic the soil-atmospheric boundary layer behavior characteristic of micrometeorology near the ground. Additional work is ongoing to analyze other geographical weather scenarios and mine emission rates with comparison to field chemical residues and mine dog performance test results.

6.0 References

Arya, S.P., 1988, *Introduction to Micrometeorology*, Academic Press, San Diego.

Bejan, A., 1995, *Convection Heat Transfer*, 2nd Edition, John Wiley & Sons, New York.

Braud, I., Dantas-Antonio, A.C., Vauclin, M., Thony, J.L., and Ruelle, P., 1995, "A Simple Soil-Plant-Atmosphere Transfer model (SiSPAT): development and field verification," *J. Hydrol.*, 166:213-250.

Braud, I., 1996, SiSPAT User's Manual, Version 2.0, LTHE, October 1996, 83 pp. (available from LTHE, B.P. 53, 38041 Grenoble, Cedex 0, France)

Bristow, K., and Campbell, G., 1984, "On the relationship between incoming solar radiation and daily minimum and maximum temperature, *Agric. For. Meteorol.*, 31:159-166.

Brutsaert, W., 1984, *Evaporation into the Atmosphere: Theory, History, and Applications,* D. Reidel, Boston.

Campbell, G.S., 1985, *Soil Physics with Basic: Transport Models for Soil-Plant Systems*, Elsevier, Amsterdam.

Campbell, G.S., and Norman, J.M., 1998, *An Introduction to Environmental Biophysics,* 2nd Edition, Springer, New York.

Carsel, R.F., and Parrish, R.S., 1988, "Developing joint probability distributions of soil water retention characteristics," *Water Resourc. Res.*, 24:755-769.

Crawford, K.C., and Hudson, H.R., 1973, "The diurnal wind variation in the lowest 1500 feet in Central Oklahoma: June 1966-May 1967," *J. Applied Meteorol.*, 12:127-132.

deMarsily, G., 1986, *Quantitative Hydrogeology – Groundwater Hydrology for Engineers*, Academic Press, San Diego.

Donatelli, M., 2002, RadEst Version 3.00, http:/www.isci.it/tools.

Dullien, F.A.L., 1992, *Porous Media Fluid Transport and Pore Structure*, 2nd Edition, Academic Press, Inc., San Diego.

Edlefsen, N.E., and Anderson, A.B.C., 1943, "Thermodynamics of Soil Moisture," *Hilgardia*, 15:31-298.

Fayer, M.J., 2000, UNSAT-H Version 3.0: Unsaturated Soil Water and Heat Flow Model Theory, User Manual, and Examples, PNNL-13249, Pacific Northwest National Laboratory, Richland, Washington.

Jury, W.A., Spencer, W.F., and Farmer, W.J., 1983, "Behavior Assessment Model for Trace Organics in Soil: I. Model Development," *J. Environ. Qual*, 12:558-564.

Jury, W.A., Spencer, W.F., and Farmer, W.J., 1984, "Behavior Assessment Model for Trace Organics in Soil: IV. Review of Experimental Evidence," *J. Environ. Qual*, 13:580-586.

Leggett, D.C., Cragin, J.H., Jenkins, T.F., and Ranney, T.A., 2001, Release of Explosive-Related Vapors from Landmines, U.S. Army Engineer Research and Development Center – Cold regions Research and Engineering Laboratory, ERDC-CRREL Technical Report TR-01-6, Hanover, NH.

Mahrt, L., 1981, "The early evening boundary layer transition," *Q.J.R. Meteorol. Soc.*, 107:329-343.

Meza, F., and Vargas, E., 2000, "Estimation of mean monthly solar global radiation as a function of temperature," *Agric.l For. Meteorol.*, 100:231-241.

Monteith, J.L., and Unsworth, M.H., 1990, *Principles of Environmental Physics,* 2nd Edition, Edward Arnold, London.

Ong, S.K., Culver, T.B., Lion, L.W., and Shoemaker, C.A., 1991, "Effects of soil moisture and physical-chemical properties of organic pollutants on vapor-phase transport in the vadose zone," *J. Contam. Hydrol.*, 11:272-290.

Pella, P.A., 1977, "Measurement of the vapor pressures of TNT, 2,4-DNT, 2,6-DNT, and EGDN," *J. Chem. Thermodynamics*, 9:301-305.

Petersen, L.W., Moldrop, P., El-Farhan, Y.H., Jacobsen, O.H., Yamaguchi, T., and Rolston, D.E., 1995, "The Effect of Moisture and Soil Texture on the Absorption of Organic Vapors," *J. Environ. Qual.* 24:752-759.

Phelan, J.M., and Barnett, J.L., 2001a, Phase Partitioning of TNT and DNT in Soils, SAND2001-0310, Sandia National Laboratories, Albuquerque, NM.

Phelan,J.M., and Barnett, J.L., 2001b, Solubility of 2,4-Ninitrotoluene and 2,4,6-Trinitrotoluene in Water, J. Chem. Eng. Data, Mar/Apr 2001.

Phelan, J.M., Gozdor, M., Webb, S.W., and Cal, M., 2000, "Laboratory Data and Model Comparisons of the Transport of Chemical Signatures From Buried Landmines/UXO" in *Detection and Remediation Technologies for Mines and Minelike Targets V*, A.C. Dubey, J.F. Harvey, J.T. Broach, R.E. Dugan, eds, Proceedings of SPIE.

Phelan, J.M., Webb, S.W., Gozdor, M., Cal, M., and Barnett, J.L., 2001, ""Effect of Soil Wetting and Drying on DNT Vapor Flux – Laboratory Data and T2TNT Model Comparisons," in *Detection and Remediation Technologies for Mines and Minelike Targets VI*, A.C. Dubey, J.F. Harvey, J.T. Broach, R.E. Dugan, eds, Proceedings of SPIE.

Phelan, J.M., Romero, J.V., Barnett, J.L., Griffin, F.A., and Parker, D.R., 2002, Landmine Chemical Signatures – PMN Mine Emission Test Results, SAND2002-3308, Sandia National Laboratories, Albuquerque, NM.

Phelan, J.M., and Webb, S.W., 2002, Chemical Sensing for Buried Landmine – Fundamental Processes Influencing Trace Chemical Detection, SAND2002-0909, Sandia National Laboratories, Albuquerque, NM.

Pruess, K., 1991, TOUGH2 - A General-Purpose Numerical Simulator for Multiphase Fluid and Heat Flow, LBL-29400, Lawrence Berkeley Laboratory, Berkeley, CA.

Rosenblatt, D.H., Burrows, E.P., Mitchell, W.R., and Parmer, D.L., 1991, "Organic Explosives and Related Compounds," *The Handbook of Environmental Chemistry,* Volume 3, Part G, O. Hutzinger, ed., Springer-Verlag, Berlin.

Settles, G.S., and D.A. Kester, 2001, "Aerodynamic sampling for landmine trace detection," in *Detection and Remediation Technologies for Mines and Minelike Targets VI*, A.C. Dubey, J.F. Harvey, J.T. Broach, R.E. Dugan, eds, Proceedings of SPIE.

Shoemaker, C.A., Culver, T.B., Lion, L.W., and Peterson, M.G., 1990, "Analytical Models of the Impact of Two-Phase Sorption on Subsurface Transport of Volatile Chemical," *Water Resourc. Res.*, 26:745-758.

van Genuchten, M.T., 1980, "A closed-form equation for predicting the hydraulic conductivity of unsaturated soils," *Soil Sci. Soc. Am. J.*, 44:892-898.

Wallace, J.M., and Hobbs, P.V., 1977, *Atmospheric Science – An Introductory Survey,* Academic Press, New York.

Webb, S.W., 2000, "A simple extension of two-phase characteristic curves to include the dry region," *Water Resourc. Res.*, 36:1425-1430.

Webb, S.W., and Phelan, J.M., 2000, "Effect of Diurnal and Seasonal Weather Variations on the Chemical Signatures from Buried Landmines/UXO," in *Detection and Remediation*

Technologies for Mines and Minelike Targets V, A.C. Dubey, J.F. Harvey, J.T. Broach, R.E. Dugan, eds, Proceedings of SPIE.

Webb, S.W., Pruess, K., Phelan, J.M., Finsterle, S.A., 1999, "Development of a Mechanistic Model for the Movement of Chemical Signatures From Buried Landmines/UXO," in *Detection and Remediation Technologies for Mines and Minelike Targets IV*, A.C. Dubey, J.F. Harvey, J.T. Broach, R.E. Dugan, eds, Proceedings of SPIE, Vol. 3710, pp. 270-282.

White, F.M., 1974, *Viscous Fluid Flow,* McGraw-Hill, New York.

Distribution

External

Havard Bach
Geneva International Center for Humanitarian Demining
Av. de la Paix 7 bis, PO Box 1300
1211 Geneva 1, Switzerland

Ian McLean
Geneva International Center for Humanitarian Demining
Av. de la Paix 7 bis, PO Box 1300
1211 Geneva 1, Switzerland

Internal

MS-0719 S.M. Howarth, 6131
MS-0719 J.M. Phelan, 6131 (10)
MS-0719 S.W. Webb, 6131 (10)
MS-0701 P.B. Davies, 6100
MS-0701 W.R. Cieslak, 6100
MS-0703 M.A. Modesto-Beato, 6218
MS-9018 Central Technical Library, 8945-1
MS-0899 Technical Library, 9616 (2)
MS-0612 Review and Approval Desk, 9612 for DOE/OSTI